HHS Public Access

Author manuscript

*Neuroimage*. Author manuscript; available in PMC 2021 January 02.

Published in final edited form as:

*Neuroimage*. 2020 December ; 223: 117347. doi:10.1016/j.neuroimage.2020.117347.

# Implicating causal brain imaging endophenotypes in Alzheimer's disease using multivariable IWAS and GWAS summary data

**Katherine A. Knutson**, **Yangqing Deng**, **Wei Pan**[2,1,*]

Division of Biostatistics, University of Minnesota, Minneapolis, Minnesota United States

## Abstract

Recent evidence suggests the existence of many undiscovered heritable brain phenotypes involved in Alzheimer's Disease (AD) pathogenesis. This finding necessitates methods for the discovery of causal brain changes in AD that integrate Magnetic Resonance Imaging measures and genotypic data. However, existing approaches for causal inference in this setting, such as the univariate Imaging Wide Association Study (UV-IWAS), suffer from inconsistent effect estimation and inflated Type I errors in the presence of genetic pleiotropy, the phenomenon in which a variant affects multiple causal intermediate risk phenotypes. In this study, we implement a multivariate extension to the IWAS model, namely MV-IWAS, to consistently estimate and test for the causal effects of multiple brain imaging endophenotypes from the Alzheimer's Disease Neuroimaging Initiative (ADNI) in the presence of pleiotropic and possibly correlated SNPs. We further extend MV-IWAS to incorporate variant-specific direct effects on AD, analogous to the existing Egger regression Mendelian Randomization approach, which allows for testing of remaining pleiotropy after adjusting for multiple intermediate pathways. We propose a convenient approach for implementing MV-IWAS that solely relies on publicly available GWAS summary data and a reference panel. Through simulations with either individual-level or summary data, we demonstrate the well controlled Type I errors and superior power of MV-IWAS over UV-IWAS in the presence of pleiotropic SNPs. We apply the summary statistic based tests to 1578 heritable imaging derived phenotypes (IDPs) from the UK Biobank. MV-IWAS detected numerous IDPs as



*Corresponding author. panxx014@umn.edu (W. Pan).

[1]for the Alzheimer's Disease Neuroimaging Initiative

[2]Data used in preparation of this article were obtained from the Alzheimer's Disease Neuroimaging Initiative (ADNI) database (adni.loni.usc.edu). As such, the investigators within the ADNI contributed to the design and implementation of ADNI and/or provided data but did not participate in analysis or writing of this report. A complete listing of ADNI investigators can be found at: http://adni.loni.usc.edu/wp-content/uploads/how_to_apply/ADNI_Acknowledgement_List.pdf

CRediT authorship contribution statement

**Katherine A. Knutson:** Data curation, Formal analysis, Investigation, Methodology, Software, Validation, Visualization, Writing - review & editing. **Yangqing Deng:** Methodology, Investigation, Writing - review & editing. **Wei Pan:** Conceptualization, Funding acquisition, Investigation, Methodology, Project administration, Resources, Supervision, Writing - review & editing.

Supplementary material

Supplementary material associated with this article can be found, in the online version, at doi: 10.1016/j.neuroimage.2020.117347.

Code and Data Availability

UK Biobank GWAS summary data for all 3144 IDPs are publicly available at http://big.stats.ox.ac.uk/about. AD GWAS summary statistics from IGAP can be downloaded at http://web.pasteur-lille.fr/en/recherche/u744/igap/igap_download.php. GWAS summary data for seven subcortical volumes from the ENIGMA network can be found at http://enigma.ini.usc.edu/research/download-enigma-gwas-results/. The 1000 genomes reference panel data is available at https://www.internationalgenome.org/data. All resting state fMRI measures can viewed using the browsers provided at https://www.fmrib.ox.ac.uk/ukbiobank/. A detailed analysis pipeline and relevant code for our summary statistic application can be found at https://github.com/kathalexknuts/MVIWAS.

possible false positives by UV-IWAS while uncovering many additional causal neuroimaging phenotypes in AD which are strongly supported by the existing literature.

**Keywords**

Causal inference; Genetic pleiotropy; Instrumental variable; Mendelian randomization; MRI; MV-IWAS; TWAS

## 1. Introduction

Alzheimer's Disease (AD) is a genetically complex disorder characterized by a collection of physiological brain changes, including many heritable phenotypes that are detectable via Magnetic Resonance Imaging (MRI) (Wenk, 2003), (Matsuda, 2017). However, recent research indicates that AD pathogenesis involves many more regions of the brain than previous realized (Frozza et al., 2018). As such, a more thorough understanding of the genetically-regulated structural and functional brain changes that drive AD progression is important for further characterization of the disease and development of targeted therapies for AD associated phenotypes.

Advances toward high-speed and affordable genotyping and multimodal imaging technologies has facilitated the collection of these data for large-scale studies, such as the Alzheimer's Disease Neuroimaging Initiative (ADNI) and UK Biobank (UKBB). Accordingly, powerful methods for integrating genetic and summarized brain measures (such as regional volumes) to test for causal imaging ROIs in AD are increasingly important (Pluta et al., 2018), (Shen and Thompson, 2020). Some existing approaches include Mendelian Randomization (MR) and the univariate Imaging Wide Association Study (UV-IWAS) (Davey Smith and Ebrahim, 2008), (Xu et al., 2017), (Zhao et al., 2019a), (Zhao et al., 2019b), (Gamazon et al., 2015), (Pluta et al., 2017). The latter method, which will be a focus of this work, is an adaptation of the popular Transcriptome Wide Association Study (TWAS) that uses a summarized imaging measure in place of gene expression to uncover possibly causal brain imaging phenotypes in neurodegenerative diseases (Gusev et al., 2016).

In our previous study, we tested the AD associations of 1578 heritable UKBB brain imaging derived phenotypes (IDPs) using summary statistic based univariate Mendelian Randomization (MR), UV-IWAS, and the related univariate aSPU test (Knutson and Pan, 2020), (Pan, 2009), (Pan et al., 2015). We identified ten significant IDPs by UV-IWAS tests, proffering a set of endophenotypes with putative causal effects on AD under satisfaction of key modeling assumptions (Wainberg et al., 2019). One of these assumptions, which is required for consistent estimation of causal effects, is that the SNPs used in the IWAS model (as instrumental variables, IVs) only affect AD by means of the endophenotype being tested. This so-called"exclusion restriction" is violated if any SNP demonstrates horizontal genetic pleiotropy, the phenomenon in which a variant affects multiple causal intermediate risk phenotypes. The presence of pleiotropic variants in univariate IV-analysis can ultimately lead to inflated Type I error rates and inadequate statistical power, as is later demonstrated in UV-IWAS through simulations. These consequences have warranted skepticism toward the

results of univariate MR methods and has motivated the development of tests, such as MR-PRESSO and the heterogeneity Q-test, to identify and correct for pleiotropic instruments in univariate MR (Pickrell, 2015), (Verbanck et al., 2018), (DelGreco et al., 2015), (Bowden et al., 2019), (Schaid et al., 2016). In particular, it has been shown that there are wide-spread pleiotropic effects of SNPs across the genome.

In this study, we consider a multivariate extension of the univariate IWAS model, namely MV-IWAS, which provides consistent causal effect estimates in the presence of pleiotropic variants by accounting for multiple potential intermediate pathways. This approach is closely related to the existing Multivariable Mendelian Randomization IVW regression (MV-MR IVW), as outlined by Burgess and Thompson (Burgess and Thompson, 2015). We propose an extension to the MV-IWAS model which incorporates variant-specific random effects to quantify the remaining pleiotropy not captured by those phenotypes in the multivariate model. We call this approach MV-IWAS-Egger due it's similarity to MR-Egger regression (Rees et al., 2017). In addition to correcting for pleiotropic pathways, MV-IWAS can boost power by adjusting for risk phenotypes which are *not* influenced by pleiotropic SNPs in the multivariate model. We apply MV-IWAS to the individual level data of 14 brain ROIs from ADNI and identify 2 endophenotypes with causal effects on AD, namely the left hippocampus and right inferior temporal cortex volumes. We further propose a practical extension to the MV-IWAS model that depends solely on endophenotype and AD GWAS summary statistics and an external reference panel of similar ancestry. This approach accounts for the LD-structure of a set of possibly correlated SNPs, making it advantageous over the existing summary statistic based MV-MR method which is restricted to a set of strictly independent instruments (Burgess and Thompson, 2015), (Eleanor Sanderson and Borden, 2019). As shown in our previous work (Knutson and Pan, 2020), using multiple correlated SNPs (as IVs) often improves statistical power over using only independent SNPs as in MR. We validate the summary statistic based MV-IWAS via simulations. Our simulations also reveal the improved performance of MV-IWAS-Egger over the related MV-MR-Egger regression for detecting remaining pleiotropic effects. We apply this method to the publicly available summary data from UKBB and IGAP and compare these results against those from univariate IWAS tests. Finally, we validate the results of our UKBB application using the GWAS summary data of seven subcortical volumes from the ENIGMA project.

## 2. Methods

### 2.1. TWAS In the 2SLS framework

The Transcriptome Wide Association Study (TWAS) is a popular approach for inferring the causal effect of an endophenotype, typically gene expression, on a disease trait. Statistically, TWAS is an application of the 2-Stage Least Squares (2SLS) method, an instrumental variable (IV) technique that accounts for latent confounding in association testing. The assumed true model under the TWAS framework is given in Eqs. 1a and 1b, where $\epsilon_X = U\gamma_X + e_X$ and $\epsilon_Y = U\gamma_Y + e_Y$. Here, $U$ represents a set of confounders acting on the endophenotype ($X$) and disease ($Y$), and $e_X$ and $e_Y$ are random errors. Since $U$ is *unobserved*, the working model from which standard OLS estimation proceeds is a simple

regression of $Y$ on $X$ (i.e. estimating $\beta$ in Eq. 1b while ignoring the confounders embedded in the error term). The resulting effect estimates are inconsistent due to the correlation between $X$ and $\epsilon_Y$. Note that, throughout this paper, for simpler notation we drop out the intercept term in a linear regression model by assuming that the data have been suitably standardized (to have a zero-intercept).

$$X = Z\alpha + \epsilon_X \tag{1a}$$

$$Y = X\beta + \epsilon_Y \tag{1b}$$

The 2SLS/TWAS approach circumvents this problem by using a set of SNPs ($Z$) as valid instrumental variables, which are defined by the 3 key assumptions illustrated in Fig. 1a (Labrecque and Swanson, 2018). Explicitly, Z represents a matrix of SNP genotypes, with the jth column corresponding to the effect-allele counts (0, 1, or 2 for the additive model) of variant j for n subjects. The first assumption (*relevance*) requires correlation between $Z$ and $X$, and is generally maintained by selecting a set of SNPs that are associated with the endophenotype. The second assumption prohibits associations between SNPs and the confounders $U$. The third IV assumption, often referred to as the "Exclusion Restriction", requires that the only pathway by which the SNPs affect disease passes through the endophenotype being tested. This last assumption may be violated due to horizontal genetic pleiotropy, the phenomenon by which a genetic locus affects multiple intermediate phenotypes causal to disease. As such, a method to control for potential pleiotropic pathways is desirable. One such approach is a multivariate extension to the univariate TWAS method, as to be described in the coming sections.

## 2.2. The univariate IWAS model with genetic pleiotropy

The 2SLS method is so-called because it is performed in 2 stages, as given in Eq. 2a and 2b. In the first stage, the endophenotype is regressed on SNPs (as IVs) to obtain an "imputed" endophenotype, $\widehat{E[X \mid Z]} = Z\hat{\alpha} = \hat{X}$, namely the fitted values of the Stage 1 model. In Stage 2, the disease is regressed on the imputed trait, which represents the "genetically-regulated" component of the endophenotype. Explicitly, in Stage 2 we model $E[Y \mid Z] = E[X \mid Z]\beta$ (using IV assumption 2), where $E[X|Z]$ is estimated in Stage 1. If $X$ is specified as a neuroimaging phenotype, as considered in this study, the resulting approach is referred to as the univariate *Imaging Wide Association Study* (IWAS) (Xu et al., 2017). IWAS is mathematically identical to the existing TWAS/2SLS model and differs only in its application. A Wald test for $H_0{:}\,\beta = 0$ in the Stage 2 IWAS model tests the causal effect of the genetically-regulated component of an imaging endophenotype on $Y$, which is typically specified as a complex trait (such as AD).

$$X = Z\alpha + \epsilon_X \ (Stage\ 1) \tag{2a}$$

$$Y = \widehat{X}\beta + \epsilon_Y \ (Stage\ 2) \tag{2b}$$

The consistency achieved by 2SLS does not hold if a GLM is used in Stage 2, such as with logistic regression for a binary disease trait (Xue and Pan, 2019). While alternative IV approaches with superior properties for binary or nonlinear outcomes have been proposed, in this study we simply model dichotomous traits in a linear Stage 2 to adhere to the standard MR/TWAS/IWAS framework (Uddin et al., 2015), (Burgess et al., 2014), (Newey, 2013), (Amemiya, 1974), (Johnston et al., 2008). As shown previously (Xue and Pan, 2019) and to be shown through simulations to follow, due to small genetic effects, a logistic regression model can be well approximated by a linear model.

As previously discussed, the utility of TWAS (and thereby IWAS) for causal inference and consistent estimation relies on satisfaction of the IV assumptions for all Stage 1 SNPs. Violations of the exclusion restriction in univariate IWAS due to horizontal genetic pleiotropy can be shown mathematically by decomposing the Stage 2 error term (Eq. 2b) into two components, $\epsilon_Y = C\gamma_C + e_Y$, where $e_Y$ represents the random error and C represents the set of r − 1 intermediate phenotypes (excluding $X$) with genetically regulated effects on $Y$. Without accounting for these intermediate pathways in Stage 2, $\hat{\beta}$ is inconsistent due to pleiotropy-induced correlation between $\widehat{X}$ and $C$. This challenge motivates the multivariate IWAS model, an extension of the univariate model that adjusts for multiple genetically regulated disease pathways.

### 2.3. The multivariable IWAS model

The multivariable IWAS model (MV-IWAS), given by the system of equations in 3, is a straightforward multiple linear regression extension of UV-IWAS (Lin et al., 2015), (Barbeira et al., 2019). In Stage 1, $r$ endophenotypes with putative disease associations are imputed, with the kth endophenotype given by $\widehat{X}_k = Z^{(k)}\hat{\alpha}_k$ for all $k \in 1, \ldots, r$. Each Stage 1 model uses an endophenotype-specific set of SNPs, $Z^{(k)}$ of dimension $n$ by $p_k$. We define p to be the total number of unique SNPs used across all $k$ endophenotypes. The multivariate Stage 2 model incorporates all $r$ imputed endophenotypes, thereby adjusting for possible pleiotropic pathways from SNPs-to-disease. For an appropriately chosen set of Stage 1 traits, this model will yield consistent estimates of an endophenotype's genetically regulated causal effect on disease $\left(\hat{\beta}_k\right)$. In the case that endophenotypes which are *not* influenced by pleiotropic variants but are reasonably predictive of the disease are included in Stage 2, MV-IWAS will gain efficiency over the univariate test by reducing the residual variance.

$$\begin{cases} X_1 = Z^{(1)}\alpha^{(1)} + \epsilon^{(1)} \\ \quad\vdots \\ X_r = Z^{(r)}\alpha^{(r)} + \epsilon^{(r)} \\ Y = \widehat{X}_1\beta_1 + \cdots + \widehat{X}_r\beta_r + \epsilon_Y \end{cases} \tag{3}$$

The least squares estimates for $\beta$ and $Var(\beta)$ are given in Eqs. 4a and 4b, where $\sigma^2$ is the residual variance and Z is an $n \times p$ matrix of genotypes for all Stage 1 SNPs, i.e., the union of SNPs represented in $Z^{(1)}, \ldots, Z^{(r)}$. $W$ represents the $p \times r$ matrix of SNP effect estimates of the $r$ endophenotypes, where the kth column includes all $p_k$ estimates of $\alpha^{(k)}$ and zero entries for all $p - p_k$ SNPs not includes in the Stage 1 model for endophenotype k. If the Stage 1 SNP-sets for all r endophenotypes are disjoint (i.e. each of the p SNPs only used to impute 1 phenotype), W will be a block diagonal matrix with r blocks. The case in which the samples used to estimate $\alpha_k$ (stage 1) and $\beta$ (stage 2) come from different studies is referred to as "2-Sample" MV-IWAS, which is often a more convenient alternative to the one-sample case when disease and endophenotype data are not available from the same study.

$$\hat{\beta} = \left(W^T Z^T Z W\right)^{-1} W^T Z^T Y \tag{4a}$$

$$\widehat{Var}(\hat{\beta}) = \left[W^T Z^T Z W\right]^{-1} \hat{\sigma}^2 = \left[W^T Z^T Z W\right]^{-1} \frac{Y^T Y - \hat{\beta}^T W^T Z^T Y}{n - r} \tag{4b}$$

OLS standard error estimation for IWAS assumes uncorrelated and homoscedastic errors. The former is generally upheld by strictly limiting analyses to a set of unrelated subjects, where relatedness can be determined by self-report or, more rigorously, using existing statistical methods for relationship inference based on genotype data (Manichaikul et al., 2010). The latter assumption, namely $Var\left(\epsilon_Y \mid \hat{X}\right) = \sigma^2 I_n$, will be violated for binary outcomes using OLS, yielding biased estimates for $Var(\hat{\beta})$. Even so, our simulations reveal comparable performance (type I errors, power, and coverage) for continuous and binary outcomes, suggesting that the least squares approach may still be approximately valid for dichotomous traits in the current application. Existing studies have proposed the use of robust standard errors to allow for heteroscedasticity in 2SLS, a possible direction for future work in MV-IWAS (Pacini and Windmeijer, 2016),(Baiocchi et al., 2014).

### 2.4. Accounting for remaining directional pleiotropy with MV-IWAS-Egger

The above formulation achieves consistent causal estimation of endophenotype effects when all pleiotropic pathways from Z to Y are captured through $X_1, \ldots, X_r$. However, accounting for all intermediate pathways is unrealistic for complex diseases, as some may be unknown or unmeasured. What's more, as predictive power for each endophenotype is improved by increasing the number of Stage 1 SNPs, the probability that any one variant affects AD through an unrepresented phenotype is high. Here, we extend the Stage 2 model in Eq. 3 to account for residual genetic effects on Y above those mediated by the set of $X_k$, as illustrated in Fig. 1c. Specifically, we incorporate variant-specific random effects $\tau_j \overset{\text{i.i.d.}}{\sim} N\left(\mu, \sigma_\tau^2\right)$, where $\mu$ represents the mean pleiotropic effect across all p SNPs (Eq. 5a). Under the regression equation in 5b, we can estimate and test for both endophenotype-specific causal effects ($H_0: \beta_k = 0$) *and* the presence of remaining directional pleiotropy ($H_0: \mu = 0$). Here, $Z_i$ represents the p-vector of genotypes for subject i.

$$Y_i = \sum_{j=1}^{p} Z_{i,j}\tau_j + \widehat{X}_{i,1}\beta_1 + \cdots + \widehat{X}_{i,r}\beta_r + \epsilon_{i,Y} \tag{5a}$$

$$E\left[Y_i \mid Z, \widehat{X}\right] = Z_i(\mathbb{1})\mu + \widehat{X}_{i,1}\beta_1 + \cdots + \widehat{X}_{i,r}\beta_r \tag{5b}$$

OLS estimation of $[\beta, \mu]^T$ is equivalent to the MV-IWAS estimates given in 4a after replacing W with $[(\mathbb{1}), W]$, where $(\mathbb{1})$ is a p-vector of ones. To estimate their corresponding variances using OLS, we rely on the following approximation: $Var\left(Y_i \mid Z_i, \widehat{X}\right) = Z_i Var\left(\tau \mid Z_i, \widehat{X}\right) Z_i^T + Var\left(\epsilon_{i,Y} \mid Z_i, \widehat{X}\right) = \sigma_\tau^2 \sum_{j=1}^{p} Z_{i,j}^2 + \sigma_Y^2 = \sigma_i^2 \approx \sigma^2$. This simplification assumes that $\sum_{j=1}^{p} Z_{i,j}^2$ is constant across subjects, which is particularly unrealistic for small p. However, it is reasonable to expect that $\sigma_\tau^2 << \sigma_Y^2$, since each common variant explains a small proportion of the total disease heritability in complex disease (and made even smaller after removing the proportion explained via the adjusted intermediate phenotypes). Therefore, approximating $\sigma_i^2$ by $\sigma^2$ will likely be valid in practice. We assess the validity of this approach for various relative magnitudes $\sigma_\tau^2$ and $\sigma_Y^2$ through simulation. Variance estimates are then approximated as

$$\begin{aligned} \widehat{Var}\left([\beta, \mu]^T\right) &\approx \left([(\mathbb{1}), W]^T Z^T Z [(\mathbb{1}), W]\right)^{-1} \hat{\sigma}^2 \\ &= \left([(\mathbb{1}), W]^T Z^T Z [(\mathbb{1}), W]\right)^{-1} \frac{Y^T Y - [\beta, \mu]^T [(\mathbb{1}), W]^T Z^T Y}{n - r - 1}, \end{aligned} \tag{6}$$

which closely resembles the MV-IWAS estimates in 4b. By adjusting for additional pleiotropic genetic effects, MV-IWAS-Egger estimates are expected to be less biased than under the original MV-IWAS model. However, the original approach will have greater efficiency (and thereby power) if there are no additional SNPs-to-disease pathways above those included in the model. Additionally, in anomalous cases where $\sigma_\tau^2$ is relatively large, $Var([\beta, \mu]^T)$ will be underestimated using the residual variance approximation in MV-IWAS-Egger, again yielding some loss of efficiency.

### 2.5. MV-IWAS Using GWAS summary statistics

Given individual level genotype, endophenotype, and disease trait data, the OLS estimates in Eqs. 4a and 4b and their MV-IWAS-Egger counterparts are straightforward to compute. However, concerns of patient privacy often limits access to these data. As such, we desire an extension of the MV-IWAS model that depends only on publicly available GWAS summary statistics, possibly from different studies, and an external reference panel. We outline such an approach in the following section, which parallels the method proposed by Deng and Pan (Deng and Pan, 2017a), (Deng and Pan, 2017b), (Yang et al., 2012). Through simulation, we evaluate this model under both the one and two sample cases (i.e. disease and endophenotype GWAS from the same sample versus different samples of similar ancestry).

Without individual level data, the quantities $Z^TZ$, $Z^TY$ and $Y^TY$ are unknown and must be estimated. Henceforth, we refer to the sample of $n_G$ subjects from the disease-trait GWAS as the "disease-GWAS sample", and denote the genotype matrix of $n_R$ subjects from a reference sample of similar ancestry by $Z_R$. For a normalized genotype matrix, sufficiently large sample size and a homogeneous population, $Z^TZ$ can be estimated using a reference panel of similar ancestry as

$$\frac{Z^TZ}{n_G} \approx \frac{Z_R^TZ_R}{n_R} \quad \rightarrow \quad \widehat{Z^TZ} = \frac{n_G}{n_R}Z_R^TZ_R\,. \tag{7}$$

In the following section, we discuss some guidelines for estimating this quantity. Estimation of $Z^TY$ relies on the marginal SNP effect estimates on the disease trait, as reported in GWAS summary statistics. We denote the jth SNP's genotypes as $Z_j$ (n × 1) and it's effect on $Y$ as $\alpha_j^{(Y)}$, which is estimated by $\hat{\alpha}_j^{(Y)} = \left(Z_j^TZ_j\right)^{-1}Z_j^TY$ with variance $\widehat{Var}\left(\hat{\alpha}_j^{(Y)}\right) = \frac{\left[Y^TY - \hat{\alpha}_j^{(Y)}Z_j^TY\right]}{n_G-1}\left[Z_j^TZ_j\right]^{-1}$. Estimates for each component of the p-vector $Z^TY$, denoted as $\left\{Z^TY\right\}_j$ for SNP j, directly follows from manipulation of $\hat{\alpha}_j^{(Y)}$, given by

$$\left\{\widehat{Z^TY}\right\}_j = \left(\widehat{Z_j^TZ_j}\right)\hat{\alpha}_j^{(Y)} \tag{8}$$

where $Z_j^TZ_j$ is estimated using an external reference panel as in Eq. 7.

Finally, we manipulate the marginal variance estimates for each SNP to get p estimates of $Y^TY$, given by

$$\left\{\widehat{Y^TY}\right\}_{(j)} = (n_G-1)\widehat{Z_j^TZ_j} * \widehat{Var}\left(\hat{\alpha}_j^{(Y)}\right) + \hat{\alpha}_j^{(Y)}\widehat{Z_j^TY} \tag{9}$$

for SNP j. Our final estimate of $\widehat{Y^TY}$ is obtained by taking the median value of all $\left\{\widehat{Y^TY}\right\}_{(j)}$. Plugging $\widehat{Z^TZ}$, $\widehat{Z^TY}$, and $\widehat{Y^TY}$ into Eq. 4a and 4b (or the related MV-IWAS-Egger estimates) gives MV-IWAS estimates of the genetically-regulated and pleiotropy-adjusted effects of each endophenotype based solely on GWAS summary statistics and a reference panel.

It is noted that, in our previous works on GWAS summary data-based TWAS/IWAS (Knutson and Pan, 2020; Xu et al., 2017), the tests were based on univariate/marginal Z-statistics of SNPs; here, our proposed test is based on estimating the regression coefficient $\beta$ in a joint/multivariate regression model.

### 2.6. Estimating SNP-Correlations using an external reference sample

When individual level data is not available, the choice of GWAS and corresponding reference sample for estimating SNP correlations ($Z^TZ$) can have a substantial impact on the performance of the summary statistic based MV-IWAS estimation (Deng and Pan, 2018). We expect that the SNP correlations estimated from a study sample will asymptotically

approximate the true correlation structure of an ancestrally homogeneous subpopulation. Therefore, $\widehat{Z_R^T Z_R}$ should be a consistent estimate of $\widehat{Z_G^T Z_G}$ for large GWAS and reference samples. In their 2017 exploration of LD estimation in fine-mapping experiments, Brenner et al. conclude that a reference panel of 1000 subjects is sufficient to approximate the LD-structure of GWAS sample of 5000 participants (Benner et al., 2017).

Some regularization approaches have been proposed to improve estimation of $Z_G^T Z_G$, though these techniques can not overcome the handicap of an unrepresentative or small sample (Benner et al., 2017). Deng and Pan propose a multiple imputation type approach for handling LD estimation with small sample sizes and emphasize its improved power over existing methods in some situations, such as penalization of the off-diagonal components of $Z_R^T Z_R$; $\widehat{Z_G^T Z_G} = (1 - s) Z_R^T Z^R + sI$ for some $s \in [0, 1]$ (Deng and Pan, 2018; Mak et al., 2017). We do not apply these techniques in the applications of this study, but they nonetheless warrant consideration in summary statistic based methods such as MV-IWAS.

### 2.7. Advantage of MV-IWAS over existing multivariate approaches

MV-IWAS and MV-IWAS-Egger are analogous to the existing Multivariable Inverse-Variance Weighted and Egger Regression Mendelian Randomization methods (MV-IVW, MV-Egger) using neuroimaging phenotypes, respectively (Burgess and Thompson, 2015). In fact, provided all SNPs are strictly uncorrelated, UV-IWAS is asymptotically equivalent to the IVW MR. However, the IVW and Egger estimators (and by extension their multivariate version) suffer from substantial power loss when restricted to a smaller set of independent IVs/SNPs (Hemani et al., 2018), (Bowden et al., 2016). IWAS can therefore achieve greater power over MR by leveraging a larger set of SNPs (as IVs) in moderate LD (Knutson and Pan, 2020).

Another related method is an extension of UV-IWAS to testing on multiple (neuroimaging) endophenotypes simultaneously (Xu et al., 2017). Their method improves statistical power for association using the so-called doubly adaptive sum of scores test (daSPU), which data-adaptively determines the relative contributions of the SNPs and the endophenotypes in a collapsed test statistic (Kim et al., 2016). This approach has particular utility in gene-based testing (i.e. Stage 1 SNPs chosen from within or near the coding region of a gene), where the collective information across intermediate genetic pathways boosts power for detecting disease-associated genes. However, unlike UV-IWAS and MV-IWAS, the data-adaptive test does not support causal interpretation. More importantly, as a global test (with a null hypothesis of no disease association with any of the endophenotypes), the method does not estimate the joint effects of each endophenotype after adjusting for other endophenotypes. In contrast, our proposed MV-IWAS facilitates formal inference for endophenotype-specific associations with disease. MV-IWAS is therefore a more appropriate and powerful parametric approach for uncovering *causal* genetically-regulated endophenotype-disease associations using multiple possibly correlated SNPs.

### 2.8. Applied analysis procedure

In this report, we use MV-IWAS to test for genetically regulated AD-endophenotype causal associations using both individual level and summary data from multiple cohorts. The aims of these analyses are two-fold; 1) to identify a set of MRI-derived phenotypes with causal associations in AD, with particular interest in causal IDPs that are replicable across multiple datasets and 2) to compare the IDPs identified by MV-IWAS against analogous UV-IWAS and Mendelian Randomization approaches.

Fig. 2 summarizes the three applied data analyses performed in this study. Our first application uses individual level data from the first phase of the Alzheimer's Disease Neuroimaging Initiative (ADNI1). We then apply the 2-sample summary statistic based approaches to the publicly available phase 1 GWASs of brain imaging phenotypes from UKBiobank and the AD GWAS from the International Genomics of Alzheimer's Project (IGAP). Finally, we replicate results from the UKBB application using summary data on seven subcortical volumes from the ENIGMA network. For all LD estimation, we use 503 samples of European ancestry from Phase 3 of the 1000 Genomes Project (Consortium, 2010). In the following sections, we describe each of these datasets and detail our Stage 1 model building procedures. A detailed analysis pipeline and relevant code for our summary statistic application can be found at https://github.com/kathalexknuts/MVIWAS.

### 2.9. Data

Data used in the preparation of this article were obtained from the Alzheimer's Disease Neuroimaging Initiative (ADNI) database (adni.loni.usc.edu). The ADNI was launched in 2003 as a public-private partnership, led by Principal Investigator Michael W. Weiner, MD. The primary goal of ADNI has been to test whether serial magnetic resonance imaging (MRI), positron emission tomography (PET), other biological markers, and clinical and neuropsychological assessment can be combined to measure the progression of mild cognitive impairment (MCI) and early Alzheimer's disease (AD). For up-to-date information, see www.adni-info.org.

ADNI1 has collected clinical, biomarker, and imaging data from 200 AD diagnosed patients, 400 mild cognitive impaired (MCI) patients, and 200 cognitively normal (CN) patients at baseline (Saykin et al., 2015). We only consider the 735 individuals who have both phenotype and genotype data (172 AD, 211 Cognitively Normal, 352 Mild Cognitive Impairment) and exclude subjects who self identify as Latino or His-panic. We categorize all MCI and CN patients as "non-AD" cases. We consider the baseline gray matter volumes from 14 brain ROIs with suggestive roles in AD, as used in the study of Xu et al. (2017). Specifically, we consider the left and right volumes of the Inferior Parietal, Inferior Temporal, Medial Orbitofrontal, Parahippocampal, Precuneus, Posterior Cingulate, and Hippocampal regions. As to be discussed, we adjust our analysis for the potential confounders of age, gender, handedness, education level and intracranial volume at baseline. We perform genetic imputation using the 1000 Genomes Project (1000G) Phase 3 reference panel using the SHAPEIT (for pre-phasing) and IMPUTE2 software. We filter out SNPs with MAF $< 0.05$ and $R^2 > 0.8$, leaving 6,286,276 remaining variants.

The UK Biobank (UKBB) is a large-scale prospective cohort study with phenotype and genetic data on ~ 500,000 subjects, and additional brain MRI data for a smaller subset of participants (projected 100,000 subjects by 2022). In 2018, Elliott et al. reported GWAS summary statistics at 11,734,353 SNPs for 1578 heritable brain imaging phenotypes (IDPs), including 306 functional, 656 diffusion, and 616 structural MRI measures (Elliott et al., 2018). These round 1 GWASs were based on the data from 8428 UKBB participants. Preceding association testing, all IDPs were quantile normalized, outliers were removed, and the following set of confounders were regressed out: age, sex, 4 measures of the subject's position, 2 measures of head motion, volumetric head size, the top 40 genetic PCs, and 10 "drift" covariates (to account for software, hardware, or protocol changes throughout data collection). Various transformation on these covariates were also included (e.g. age$^2$), as described in (Elliott et al., 2018).

ENIGMA ("Enhancing Neuro Imaging Genetics Through Meta Analysis") is a world-wide network focused on combining imaging and genetic data for the study of brain function and disease. As part of this initiative, a 2015 study publicly reported GWAS summary data on 7 subcortical region volumes (left + right hemispheres) using 13,171 subjects (Hibar et al., 2015), (Wu, 2020). These ROIs include the nucleus accumbens, caudate, putamen, pallidum, amygdala, hippocampus and thalamus, with volumes all correct for ICV.

For AD information, we use summary statistics from the International Genomics of Alzheimer's Project (IGAP) (Lambert et al., 2013). IGAP is a large two-stage study based upon genome-wide association studies (GWAS) on individuals of European ancestry. In stage 1, IGAP used genotyped and imputed data on 7,055,881 single nucleotide polymorphisms (SNPs) to meta-analyse four previously-published GWAS datasets consisting of 17,008 Alzheimer's disease cases and 37,154 controls (The European Alzheimer's Disease Initiative (EADI), the Alzheimer's Disease Genetics Consortium (ADGC), The Cohorts for Heart and Aging Research in Genomic Epidemiology consortium (CHARGE), The Genetic and Environmental Risk in AD consortium (GERAD)). In stage 2, 11,632 SNPs were genotyped and tested for association in an independent set of 8572 Alzheimer's disease cases and 11,312 controls. Finally, a meta-analysis was performed combining results from stages 1 and 2.

### 2.10. Stage 1 model selection

To select Stage 1 SNPs for the 14 ADNI1 endophenotypes with individual level data, we implement a multistep approach that accounts for possible confounders of the endophenotype-AD relationship. We first perform LD pruning to remove loci based on high pairwise LD ($R^2 > 0.8$), retaining the SNP with the highest MAF in each pair. Chromosomes 2 and 22 correspond to the largest and smallest post-pruning genotype matrices with 95,431 and 16,150 SNPs, respectively. Next, we regress each endophenotype on baseline measures for age, gender, handedness, education level and intracranial volume. Using the residuals from this first stage as an outcome and genotype matrix, we fit an elastic net for each chromosome separately, with $\alpha = 0.5$ (i.e. equal importance assigned to L1 and ridge penalties) and the regularization parameter ($\lambda$) chosen based on minimum 5-fold CV error. We retain all SNPs with non-zero coefficients and estimate their joint effects in a multiple

linear regression using SNPs across all chromosomes. A summary of the number of remaining SNPs for each of the 14 endophenotypes is given in Table 1. The average $R^2$ between corresponding true and imputed endophenotypes is 0.5883 (min = 0.4146, max = 0.7233), demonstrating the adequate predictive power of our Stage 1 models for these data.

For summary statistic based MV-IWAS using UKBB IDPs, we use LD clumping and thresholding on each endophenotype GWAS to select variants. For each of the 1578 heritable IDPs, we perform LD Clumping using the 1000 Genomes reference panel (EUR) with a clumping radius of 1 Mb and $R^2$ cutoff of 0.1. In our previously published work, we implemented univariate IWAS and aSPU tests for IDP-mediated-AD associations using 3 different significance thresholds and found that the $p < 5 * 10^{-5}$ threshold yielded the greatest number of significant univariate IWAS tests. We will use this threshold for Stage 1 model selection in the present study. Across all heritable IDPs, the minimum, mean, and maximum number of Stage 1 SNPs were 43, 81, and 132, respectively.

### 2.11. Simulation framework

We conduct extensive simulation studies to assess the performance of MV-IWAS and MV-IWAS-Egger across numerous realistic scenarios, and compare these methods against UV-IWAS and, in summary data applications, MV-MR. We evaluate these approaches for both quantitative and binary disease traits under the one and two sample cases. We perform two sets of simulations, the first comparing UV- and MV-IWAS in the absence of remaining directional pleiotropy and the second evaluating all methods across varied magnitudes of the mean direct pleiotropic effect ($\mu$). In this section, we outline the set-up for these simulations.

To mimic realistic genetic data, we randomly simulate genotypes for n = 20000 subjects using LD correlations estimated directly from individual level ADNI1 data. More specifically, we generate allele frequencies from a multivariate binomial distribution (*bindata* package in R) based on the correlations of 20 genome-wide SNPs that were randomly sampled from the Stage 1 SNPs used in our application to ADNI1 data (Taudes, 2005). The LD structure for these SNPs, as estimated using ADNI1 versus 1000G, is illustrated in Figs. 3a and 3b.

For 2 sample simulations, we randomly split subjects into 2 sets of $n_1 = n_2 = 10000$ for estimating endophenotype and disease SNP effects, respectively. Using these data, we simulate 3 endophenotypes from $X_k = a_k Z + U + \epsilon_k$, where $\epsilon_k$ and $U \sim N(0, I)$. To reflect a situation in which 30% of SNPs demonstrate pleiotropic effects, we set the first 14 true effect sizes for the kth endophenotype to zero (i.e. $\alpha_{k,j} = 0$ for $j = 1, \ldots 14$), and randomly sample the remaining 6 invalid SNPs from $\alpha_{k,j} \sim 0.3^* N(0, 1)$. Across all settings, the mean SNP-heritabilities for the 3 simulated endophenotypes were 0.156, 0.100, and 0.097 (estimated as the variance of $X_k$ explained by Z). These values are comparable to the heritability of the UKBB IDPs considered in this study (mean $\hat{h}^2 = 0.29$), as estimated and publicly reported by Elliott et al. (2018).

We simulate quantitative disease traits from $Y_i = \beta_1 X_{1,i} + \beta_2 X_{2,i} + \beta_3 X_{3,i} + \beta_4 U_i + \epsilon_{Y,i}$ for $i \in 1, \ldots, n$, where $\epsilon_Y \overset{iid}{\sim} N(0, I)$. For binary disease traits, we generate Bernoulli probabilities from

$$p_i = \text{logit}^{-1}(b_0 + b_1 X_{1,i} + b_2 X_{2,i} + b_3 X_{3,i} + b_4 U_i)$$

and obtain $Y_i$ by randomly sampling from a Bernoulli distribution with probability $p_i$. Here, $b = (b_0, b_1, b_2, b_3, b_4)$ represent log odds or log odds ratios. In order to evaluate estimates from our *linear* Stage 2 working model, we rescale these log odds ratios as linear model effects using the following procedure (Pattee and Pan, 2020).

Under the logistic regression model, $E[Y_i \mid X_i, U_i] = 1/(1 + \exp\{-(b_0 + b_1 X_{1,i} + b_2 X_{2,i} + b_3 X_{3,i} + b_4 U_i)\}$. A first order multivariate Taylor Series expansion of this expression about $(b_1, b_2, b_3, b_4) = (0, 0, 0, 0)$ yields an approximate linear model, $E[Y_i \mid X_i, U_i] \approx \beta_0 + \beta_1 X_{1,i} + \beta_2 X_{2,i} + \beta_3 X_{3,i} + \beta_4 U_i$ with

$$\beta_k = \frac{e^{-b_0}}{\left(1 + e^{-b_0}\right)^2} b_k . \tag{10}$$

Later in application, we use this approach to linearize the OR from IGAP AD summary data. An approximation of $Var\left(\widehat{b_k}\right)$ can be explicitly justified using the law of total variance: $Var(\beta_k) = E\left[Var\left(\hat{\beta}_k \mid \hat{b}_0\right)\right] + Var\left[E\left(\hat{\beta}_k \mid \widehat{b_0}\right)\right] \approx \left(\frac{e^{-b_0}}{\left(1 + e^{-b_0}\right)^2}\right)^2 Var\left(\widehat{b_k}\right) + Var\left(\frac{e^{-\hat{b}_0}}{\left(1 + e^{-\hat{b}_0}\right)^2}\right) b_k^2$. Note that

$$\begin{aligned} \exp(-b_0) &= P(Y_i = 0 \mid X_i = 0, U_i = 0) / P(Y_i = 1 \mid X_i = 0, U_i = 0) \\ &\approx P(Y_i = 0) / P(Y_i = 1) \end{aligned}$$

represents the ratio of the proportions of controls and cases, again due to small genetic (and confounding) effect sizes. Then, $Var[\widehat{p_0}(1 - \widehat{p_0})] = E\left[(\hat{p}_0)^2 (1 - \hat{p}_0)^2\right] - E[\hat{p}_0(1 - \hat{p}_0)]^2 \approx 0$, yielding the linearized variance approximation given in Eq. 11.

$$Var(\beta_k) \approx \left(\frac{e^{-b_0}}{\left(1 + e^{-b_0}\right)^2}\right)^2 Var\left(\hat{b}_k\right) \tag{11}$$

In all quantitative trait simulations, we set $(\beta_1, \beta_2, \beta_3, \beta_4) = (0, 0.5, -0.2, 1)$. In binary trait simulations, we set $(b_1, b_2, b_3) = (0, 0.5, -0.5)$ and $b_0 = -\log(4) = -1.38$, which corresponds to the ratio of controls to cases in ADNI1 ($\approx 4$). After transformation, $(\beta_1, \beta_2, \beta_3) = (0, 0.08, -0.08)$. For modeling with individual level data, we estimate the joint effects $(\hat{\alpha}_{k,j})$ for each

endophenotype, impute each $\hat{X}_k$, and estimate $\hat{\beta}_1, \hat{\beta}_2,$ and $\hat{\beta}_3$ in Stage 2 using both the UV-IWAS and MV-IWAS models. As previously discussed, we assume a linear Stage 2 model for both quantitative and binary disease traits. For the summary statistic based approach, we estimate the marginal SNP effects for each endophenotype and disease, as are reported in GWAS summary statistics, and use the 1000G EUR reference panel of 503 subjects to estimate $\widehat{Z^T Z}$ for Stage 2. For all settings, we perform 1000 iterations and compare the point estimates, 95% coverage, and power across models. Note that power estimates for $\beta_1 = 0$ correspond to the Type I error rate, which will ideally be maintained near 0.05.

For our simulations which incorporate additional direct pleiotropy, we simulate variant specific effects by sampling from $\tau_j \sim N(\mu, \sigma_\tau^2)$. We compare the performance of all methods across various magnitudes of the mean pleiotropic effects, $\mu \in [0,\ 0.05,\ 0.2]$, and the proportion of each SNPs variance explained compared to $\sigma_Y^2; \sigma_\tau^2 \in [0.0025, 0.005, 0.0075, 0.01] * \sigma_Y^2$, with $\sigma_Y^2 = 1$ for all simulations. These values were chosen based on published simulations of the analogous MV-MR methods, such as in (Rees et al., 2017). The choice of $\mu = 0.2$ reflects an expected upper bound for mean variant specific effects, determined based on the rounded mean marginal SNP effect across all variants in the APOE gene in IGAP (after linear approximation). We implement MV-IVW and MV-Egger using the MendelianRandomization package in R. For these MR models only, we perform recommended LD pruning with an $R^2$ cutoff of 0.05 and retain the SNP in correlated pairs with the highest MAF based on 1000 Genomes.

## 3. Results

### 3.1. MV-IWAS Improves type-I error control compared to UV-IWAS

Our first set of simulations compared UV- and MV-IWAS in the absence of additional direct pleiotropic effects. For both quantitative and binary disease traits, Type I error rates were well-controlled for MV-IWAS using individual level data, as evaluated based on the power estimates for $\beta_1 = 0$ (Table 2). 95% simulation coverages were near the nominal level for all MV-IWAS endophenotype estimates, with notably high power for $\beta_2$ and $\beta_3$ in both the 1 and 2 sample case. The summary statistic based approach performed comparably, with well maintained but slightly more conservative Type I errors and coverages near 95%. Ultimately, these results empirically validate the summary statistic extension of the MV-IWAS model, even with a small reference panel for LD approximations.

In contrast, the Type I errors for the univariate IWAS model were highly inflated, specifically at 0.459 and 0.346 for the 2 sample models of quantitative and binary traits, respectively. 95% confidence intervals for the first 100 simulations are illustrated in Fig. 4, which highlights the increased variability in $\hat{\beta}$ for UV-IWAS that is not properly captured by the estimated variance. Power estimates for $\beta_2$ and $\beta_3$ were also substantially lower than those of MV-IWAS for both quantitative and binary diseases. These results serve to highlight the notable improvement of MV-IWAS, both using individual level data and summary statistics, over the standard univariate IWAS approach for the detection of true causal endophenotypes while controlling Type I error rates.

We further assessed the performance of MV-IWAS when one of the causal pleiotropic endophenotypes was excluded from the Stage 2 model. This situation is reasonable to expect in applications where some of the substantive pleiotropic pathways are unknown or unmeasured. For simulations of a quantitative disease trait, excluding $X_3$ in the Stage 2 model resulted in a somewhat elevated Type I error but similar power for $\beta_2$ compared to the fully specified model in Table 2 (specifically, Type I Error = 0.16 and Power = 0.989). Nonetheless, the performance of MV-IWAS with 2 of the 3 causal endophenotypes was dramatically improved over that of the univariate IWAS test, highlighting its utility in spite of some omitted causal pathways.

### 3.2. Superior performance of MV-IWAS-Egger over alternative approaches under directional pleiotropy

For our second set of simulations, we incorporated direct variant-specific pleiotropic effects and evaluated the performance of all IWAS and MR methods. Fig. 5 compares the Type I error rates and power for varied magnitudes of $\sigma_\tau^2$ with (a) $\mu = 0$, (b) $\mu = 0.05$, and (c) $\mu = 0.2$. Across all settings, both the individual level and summary statistic based applications of MV-IWAS-Egger maintained Type-I Errors below 0.05 and achieved the highest power compared to all other methods. In the case of balanced horizontal pleiotropy (i.e. $\mu = 0$), all multivariate methods had well controlled Type-I Errors for $\beta_1$ and $\mu$ (for Egger methods). However, MV-IWAS-Egger was alone able to control Type I errors in the presence of directional direct pleiotropic effects ($\mu = 0.05$ and 0.2). As may be expected, the Type-I error rates for both UV- and MV-IWAS increased with larger mean direct pleiotropic effects, and were inflated even above those for the related MV-IVW method.

In accordance with findings from our previous work (Knutson and Pan, 2020), both MR methods had substantially lower power to detect causal effects for $\beta_2$ and $\beta_3$ compared to all IWAS methods in all scenarios. This difference was particular notable for the largest direct pleiotropic effect size ($\beta = 0.2$); while the power for both $\beta_2$ and $\beta_3$ was greater than 0.8 for all IWAS models in this setting, neither of the MV-MR methods achieved power greater than 0.2 for $\beta_2$ or $\beta_3$. What's more, the test of $H_0 : \mu = 0$ for MV-MR-Egger was notably underpowered, with power of ≈ 13% for both $\mu = 0.05$ and $\mu = 0.2$. In contrast, the MV-IWAS-Egger test for directional pleiotropy was very powerful (power near 1) *and* controlled the Type-I error rate below 0.05 when $\mu = 0$. Finally, we point out that MV-IWAS-Egger yielded stable Type-I errors and power across all values of $\sigma_\tau^2$, validating the use of the OLS variance approximation. These simulations suggest that MV-IWAS-Egger should be preferred over alternative approaches for detecting true causal endophenotype-disease associations.

### 3.3. Application of MV-IWAS to 14 ADNI endophenotypes

MV-IWAS and MV-IWAS-Egger identified atrophy to the left hippocampus and right inferior temporal cortex as causal for Alzheimer's Disease. As reported in Table 3, our application of the univariate IWAS test to the individual level data of 14 volumetric ADNI measures identified 13 significant phenotypes at a Bonferonni adjusted significance level of 0. 05⁄14 = 0. 0036. Of these, only the left hippocampal and right inferior temporal cortex

volumes remained significant for both multivariate tests. Estimates between MV-IWAS and MV-IWAS-Egger were concordant, and the random direct effect in MV-IWAS-Egger was not significant, indicating no substantive directional pleiotropy in the multivariate model.

The notable differences between the univariate and multivariate IWAS estimates can possibly be attributed to the high degree of correlation between endophenotypes, which are illustrated by the heatmap in Fig. 6. Of particular note is the high correlation between the right and left volumes for the hippocampus ($R^2 = 0.677$), parahippocampus ($R^2 = 0.439$) and precuneus ($R^2 = 0.584$), which share 25, 4, and 7 Stage 1 SNPs between the two sides, respectively. This high degree of correlation and sharing of Stage 1 SNPs suggests the influence of genetic pleiotropy in the inflated Type I errors of the UV-IWAS tests, as was shown in simulation.

Causal AD-associations for the left hippocampus and right inferior temporal cortex volumes are strongly supported across the literature (Fox et al., 1996), (Galton et al., 2001), (Shen et al., 2014). In particular, many studies have shown that the left hippocampus exhibits greater atrophy (and at faster rates) compared to the right hippocampus, supporting the result that the left (and not the right) imputed hippocampal volume remained significant in the multivariate model ((Sarica et al., 2018), and references therein). Manhattan plots in Fig. 7 illustrate the genetic association patterns in Stage 1 for these two significant IDPs and provide comparisons against the Stage 1 models for analogous UKBB IDPs. Top SNPs for the left hippocampus are located within genes which have previously been shown to be over-expressed in AD hippocampal tissue, such as NR4A1 (rs2242107) and FAR2 (rs7137556) (Zhao et al., 2018), (Zhang et al., 2015). What's more, our imputation model includes 49 SNPs within chromosome 12, specifically 3 SNPs in 12q14 and 12 SNPs in 12q24, a finding which is corroborated throughout the literature *and* mirrors the association pattern for the related IDP in our UKBB summary statistic application, namely T1 FAST left hippocampus volume (Bis et al., 2012).

### 3.4. Univariate testing of 1578 UK biobank IDPs

Preceding application of our multivariate methods, we performed univariate IWAS tests for all 1578 heritable UK Biobank IDPs. A total of 94,025 unique SNPs were used in Stage 1 modeling across all IDPs, 15,036 of which were used to impute more than one IDP (Fig. 10). This result suggests possible pleiotropic effects, in addition to those caused by linkage disequilibrium between Stage 1 SNPs. For summary statistic based testing, we first converted all IGAP odds ratios and variances to linear regression estimates using the previously described approach, namely Eqs. 10 and 11, with $exp(-b_0) \approx 37154/17008$. For all IDPs, we used the median value of Eq. 9 across all 15,036 SNPs to obtain a stable estimate of $\widehat{Y^T Y} = 1.634237$. We also applied univariate MR-IVW and MR-Egger regression. In line with recommended practice, we performed LD clumping using 1000 Genomes with an $R^2$ cutoff of 0.001 and window of 10,000 kb for all MR analyses.

For the UV-IWAS and UV-IWAS-Egger tests, 216 and 210 IDPs were significant at a Bonferonni corrected significance threshold of 0.05/1578, respectively. 202 IDPs were significant under both models. These results diverge somewhat from those reported in our

previous work, in which a similar (but not equivalent) test was used based on univariate summary Z-statistics (Knutson and Pan, 2020). Of the 202 IDPs significant for both univariate tests, 36, 79, and 87 were based on functional, diffusion, and structural modalities, respectively. The mean variant-specific effect ($\mu$) deviated significantly from zero for 83 IDPs, indicating possible directional pleiotropy. In contrast, no IDPs were significant for univariate MR-IVW or Egger regression, including $\mu$ for all UV-MR Egger models. This result is consistent with our previous work and expectations: MR suffers from power loss by being restricted to a smaller set of uncorrelated variants.

### 3.5. Selecting UKBB imaging phenotypes for multivariate analyses

We implemented MV-IWAS separately for each of the imaging modalities, presupposing that the SNPs affecting brain structure, activity, and connectivity are largely distinct. For each of these tests, we included IDPs with unadjusted univariate p-values below 0.05 for either UV-IWAS or UV-IWAS-Egger (146 functional, 306 diffusion, and 279 structural). To address concerns of possible multicollinearity, we computed the correlations between these imputed phenotypes (using 1000G) within each of the modality groups. The mean pairwise correlation within the functional, diffusion, and structural MRI IDP modalities are 0.0381, 0.0490, and 0.0383, respectively (Fig. 8a). 3 pairs of imputed structural IDPs have correlations above 0.75, as shown in (Fig. 8b). For each pair, we retained the IDP with the smallest univariate p-value, namely unnormalized versus normalized T1 brain volume, Freesurfer brain segmentation volume without ventricles (from surface), and total versus right hemispheric cerebral white matter volumes. The 7 imputed dMRI IDPs illustrated in Fig. 8c have high pairwise correlations ($|\rho| > 0.75$). The biological connectivity between many of these pairs of IDPs have been previously identified in dMRI studies (specifically, the raw and not genetically imputed measures), such as the connection between the superior longitudinal fasciculus and cingulum bundle (Wu et al., 2016). Each of these ROIs have also been *separately* implicated in neurodegenerative diseases through dMRI based studies, indicating they may each play distinct and important roles in the brain and should therefore all be retained in the multivariate dMRI model (Yin et al., 2015), (Bubb et al., 2018), (Haghshomar et al., 2018), (Whitwell et al., 2010), (Walsh et al., 2011). The maximum correlation between imputed functional IDPs is 0.378, so we retain all 146 IDPs in our multivariate analysis.

### 3.6. Discovery of causal imaging phenotypes to AD using UKBB summary statistics

Across all 3 modalities, MV-IWAS identified new causal UKBB brain phenotypes which were not detected via univariate IWAS. We determine significance using a Bonferroni adjusted threshold of 0.05 divided by 729 (732 for MV-IWAS-Egger), the number of IDPs included across all modality-specific MV-IWAS models. A comparison of the significant IDPs between the UV and MV-IWAS tests are given in Fig. 11. All estimates are included in Supplementary Table 1.

MV-IWAS implicated the volumetric changes of many important structures within or functionally connected to the temporal lobe, such as the left and right amygdala, left superior temporal gyrus, and left and right middle and inferior temporal gyri (de Jong et al., 2008), (Poulin et al., 2011). Notably, the latter volumetric measure was also identified in our

application to individual level ADNI1 data, further corroborating the results of our summary statistic based approach. MV-IWAS also identified structural changes to the left and right putamen, precuneus, and insular cortices and the left parahippocampal gyrus (de Jong et al., 2008), (Jiji et al., 2013), (Pini et al., 2016), (Fathy et al., 2019). Numerous diffusion MRI measures related to the superior cerebellar peduncle, hippocampal subdivision of the cingulum, superior longitudinal fasciculus, and corona radiata were also uniquely discovered by the MV-IWAS test (Toniolo et al., 2018), (Zhang et al., 2007), (Mayo et al., 2019). 7 additional measures related to the anterior and posterior limbs of the internal capsule were also identified by MV-IWAS (Mayo et al., 2019).

Fig. 9 provides Manhattan plots and identifies top SNPs for IDPs with the greatest causal effect estimate from MV-IWAS-Egger within each modality group, namely total brain volume (structural), Mean OD in body of corpus callosum on FA skeleton (dMRI), and NET100 0780 (resting-state fMRI network edge) (Silbert et al., 2003), (Demey et al., 2015). Notably, 21 SNPs used for imputation of NET100 0780, including a top SNP rs116889766, are located within PRUNE2, a known risk gene for AD (Potkin et al., 2009). 14 Stage 1 SNPs (including multiple top SNPs) for the body of corpus callosum dMRI IDP are located within ALPK1 which has been previously associated with increased risk for multiple inflammatory diseases but *not* AD-related dementias (Ryzhakov et al., 2018), (Williams et al., 2019), (Ko et al., 2013). The top structural MRI IDP, total brain volume (freesurfer), was imputed using 25 Stage 1 SNPs located within SGIP1, including 12 genome-wide significant variants. The SGIP1 encoded protein has been implicated in cerebral amyloid angiopathy, the accumulation of amyloid proteins in the brain, which is highly characteristic of AD (Hondius et al., 2018). What's more, the top SNP for this IDP (rs560082768) is located within the FAM19A5 (also called TAFA5) gene, which has been previously associated with both AD and neuropsychiatric conditions (Herold et al., 2016), (Shahapal et al., 2019).

MV-IWAS also implicated many possible false positive univariate results. Specifically, 13 structural, 2 functional, and 23 diffusion MRI IDPs with significant UV-IWAS tests were *not* supported under the multivariate model. Interestingly, two structural MRI measures related to the thalamus (namely the left thalamus and L+R thalamus volumes) were supported by the UV-IWAS test but *not* the MV-IWAS model. Evidence in the existing literature suggests this UV-IWAS result may be a false positive; Aggleton et al. argue that structural MRI measures of total thalamic volume can not distinguish changes to the subset of nuclei associated with AD (Aggleton et al., 2016). Another notable finding is that the T2 left+right versus right-only amygdala sMRI measures were exclusively significant for UV- and MV-IWAS, respectively. Hemispheric lateralization of the amygdala has been observed in numerous AD studies, specifically implicating right amygdala atrophy in loss of emotional memory amongst AD patients (Philippi et al., 2015), (Cimino et al., 1991), (Buchanan et al., 2006), (Markowitsch et al., 2000). Our findings, which specifically implicate the right amygala in lieu of the aggregated left+right measure, are therefore well supported.

The IDPs which are exclusively significant for UV-IWAS can also be explained by their close relation to ROIs which were significant for MV-IWAS, possibly because the detected effect in the univariate model was due solely to it's association to a related causal IDP. For instance, the left posterior cingulate surface area was significant only under the univariate

model, but the closely related left posterior cingulate thickness (based on the same brain atlas) was significant for MV-IWAS.

These findings, along with our simulations, highlight the utility of MV-IWAS over UV-IWAS for controlling Type-I errors in the presence of genetic pleiotropy. No IDPs were significant for MV-MR Egger regression for any modality group. For MV-IVW, 1 diffusion, 3 structural, and 4 functional IDPs were significant, only two of which were also significant for MV-IWAS. These IDPs include the L Cerebral Peduncle (dMRI), R Intracalcarine Cortex volume, and L & R Supracalcarine Cortex volumes (sMRI).

### 3.7. Replicated MV-IWAS findings for UKBB and ENIGMA summary data

The ENIGMA project and UK Biobank each published GWAS summary data on comparable structural T1-weighted MRI based volumetric brain measures. These include the volume of left + right Nucleus Accumbens, Caudate, Putamen, Pallidum, Amygdala, Hippocampus and Thalamus. We perform MV-IWAS using these summary data separately for the two cohorts, but with the same set of Stage 1 SNPs (selected by clumping + thresholding, as before). As shown in Table 4, MV-IWAS yielded equivalent results between the two studies, specifically identifying the hippocampus and nucleus accumbens volumes as significant causal endophenotypes in AD. The two study's results differed slightly for MV-IWAS-Egger, as hippocampal volume was no longer significant for the ENIGMA cohort. Nonetheless, we feel that these results serve to validate our approach and implicate two replicable phenotypes in AD. Notably, in both MV-IWAS-Egger applications, the direct variant effects ($\mu$) were significant, indicating the presence of remaining genetic pleiotropy.

## 4. Discussion

In this study, we implemented a multivariate extension of the univariate IWAS model to test for the *causal* effects of multiple brain imaging endophenotypes in Alzheimer's Disease. We applied MV-IWAS to individual level data on 14 volumetric brain measures from the ADNI study, identifying 2 ROIs with considerable evidence of a causal effect on AD. These regions, namely the left hippocampus and right inferior temporal cortex, have been implicated in AD through multiple imaging and autopsy based studies (Lindberg et al., 2012), (Launer et al., 2001), (Convit et al., 1997), (Busatto et al., 2003). We further proposed a method for estimating MV-IWAS effects using only GWAS summary statistics and a reference panel, which we validated through simulation. These results highlighted the well controlled Type-I error rates and improved power of MV-IWAS, both the individual level and summary data versions, over UV-IWAS. Our simulations also highlight the out-performance of our proposed MV-IWAS-Egger test over all alternative approaches, including popular MV-MR methods, in the presence of direct pleiotropic SNPs. We applied this method to the summary data of 1578 imaging derived phenotypes and AD from UK Biobank and IGAP, respectively. MV-IWAS discovered multiple well-supported and biologically plausible IDPs above those identified by the univariate test and implicated many possible false positive UV-IWAS results. MV-IWAS can be further generalized to other molecular phenotypes with suspected causal effects on AD and can be applied to study causal pathways in numerous other complex diseases (Trushina et al., 2013), (Larsson and

Markus, 2017). Ultimately, the results of this study and the numerous applications for future research promote MV-IWAS as a promising method for identifying multiple endophenotypes causally associated with complex diseases.

## Supplementary Material

Refer to Web version on PubMed Central for supplementary material.

## Acknowledgements

This work was supported by NIH grants T32GM108557, R01AG065636, R01HL116720, R01GM113250 and R01GM126002, by NSF grant DMS 1711226, and by the Minnesota Supercomputing Institute at the University of Minnesota. KK was supported by a University of Minnesota MnDRIVE Fellowship.

Data collection and sharing for this project was funded by the Alzheimer's Disease Neuroimaging Initiative (ADNI) (National Institutes of Health Grant U01 AG024904) and DOD ADNI (Department of Defense award number W81XWH-12-2-0012). ADNI is funded by the National Institute on Aging, the National Institute of Biomedical Imaging and Bioengineering, and through generous contributions from the following: AbbVie, Alzheimer's Association; Alzheimers Drug Discovery Foundation; Araclon Biotech; BioClinica, Inc.; Biogen; Bristol-Myers Squibb Company; CereSpir, Inc.; Cogstate; Eisai Inc.; Elan Pharmaceuticals, Inc.; Eli Lilly and Company; EuroImmun; F. Hoffmann-La Roche Ltd and its affiliated company Genentech, Inc.; Fujirebio; GE Healthcare; IXICO Ltd.; Janssen Alzheimer Immunotherapy Research and Development, LLC.; Johnson and Johnson Pharmaceutical Research and Development LLC.; Lumosity; Lundbeck; Merck and Co., Inc.; Meso Scale Diagnostics, LLC.; NeuroRx Research; Neurotrack Technologies; Novartis Pharmaceuticals Corporation; Pfizer Inc.; Piramal Imaging; Servier; Takeda Pharmaceutical Company; and Transition Therapeutics. The Canadian Institutes of Health Research is providing funds to support ADNI clinical sites in Canada. Private sector contributions are facilitated by the Foundation for the National Institutes of Health (www.fnih.org). The grantee organization is the Northern California Institute for Research and Education, and the study is coordinated by the Alzheimers Therapeutic Research Institute at the University of Southern California. ADNI data are disseminated by the Laboratory for Neuro Imaging at the University of Southern California.

We thank the International Genomics of Alzheimer's Project (IGAP) for providing summary results data for these analyses. The investigators within IGAP contributed to the design and implementation of IGAP and/or provided data but did not participate in analysis or writing of this report. IGAP was made possible by the generous participation of the control subjects, the patients, and their families. The iSelect chips was funded by the French National Foundation on Alzheimer's disease and related disorders. EADI was supported by the LABEX (laboratory of excellence program investment for the future) DISTALZ grant, Inserm, Institut Pasteur de Lille, Universite de Lille 2 and the Lille University Hospital. GERAD was supported by the Medical Research Council (Grant n 503480), Alzheimer's Research UK (Grant n 503176), the Wellcome Trust (Grant n 082604/2/07/Z) and German Federal Ministry of Education and Research (BMBF): Competence Network Dementia (CND) grant n 01GI0102, 01GI0711, 01GI0420. CHARGE was partly supported by the NIH/NIA grant R01 AG033193 and the NIA AG081220 and AGES contract N01-AG-12100, the NHLBI grant R01 HL105756, the Icelandic Heart Association, and the Erasmus Medical Center and Erasmus University. ADGC was supported by the NIH/NIA grants: U01 AG032984, U24 AG021886, U01 AG016976, and the Alzheimer's Association grant ADGC-10-196728.

This research has been conducted using the UK Biobank Resource. We thank the authors and contributors in the analysis of Elliott et al. (2018) and the Oxford Brain Imaging Genetics (BIG) browser, including the lab of Dr. Benjamin Neale, for providing the summary data used in these analyses.

## References

Aggleton JP, Pralus A, Nelson AJD, Hornberger M, 2016 Thalamic pathology and memory loss in early alzheimer's disease: moving the focus from the medial temporal lobe to papez circuit. Brain 139 (7), 1877–1890. [PubMed: 27190025]

Amemiya T, 1974 The nonlinear two-stage least-squares estimator. J. Econom 2 (2), 105–110.

Baiocchi M, Cheng J, Small DS, 2014 Instrumental variable methods for causal inference. Stat. Med 33 (13), 2297–2340. [PubMed: 24599889]

Barbeira AN, Pividori MD, Zheng J, Wheeler HE, Nicolae DL, Im HK, 2019 Integrating predicted transcriptome from multiple tissues improves association detection. PLoS Genet. 15 (1), e1007889. [PubMed: 30668570]

Benner C, et al., 2017 Prospects of fine-mapping trait-associated genomic regions by using summary statistics from genome-side association studies. The American Journal of Human Genetics 101 (4), 539–551. [PubMed: 28942963]

Bis J, et al., 2012 Common variants at 12q14 and 12q24 are associated with hippocampal volume. Nat. Genet 44 (5), 545. [PubMed: 22504421]

Bowden J, Davey Smith G, Haycock PC, Burgess S, 2016 Consistent estimation in mendelian randomization with some invalid instruments using a weighted median estimator. Genet. Epidemiol 40 (4), 304–314. [PubMed: 27061298]

Bowden J, DelGreco F, Minelli C, Zhao Q, Lawlor DA, Sheehan NA, Thompson J, Davey Smith G, 2019 Improving the accuracy of two-sample summary-data mendelian randomization: moving beyond the NOME assumption. Int. J. Epidemiol 48 (3), 728. [PubMed: 30561657]

Bubb EJ, Metzler-Baddeley C, Aggleton JP, 2018 The cingulum bundle: anatomy, function, and dysfunction. Neurosci. Biobehav. Rev 92, 104–127. [PubMed: 29753752]

Buchanan TW, Tranel D, Adolphs R, 2006 Memories for emotional autobiographical events following unilateral damage to medial temporal lobe. Brain 129 (1), 115–127. [PubMed: 16291807]

Burgess S, Granell R, Palmer TM, Sterne JAC, Didelez V, 2014 Lack of identification in semiparametric instrumental variable models with binary outcomes. Am. J. Epidemiol 180 (1), 111. [PubMed: 24859275]

Burgess S, Thompson SG, 2015 Multivariable mendelian randomization: the use of pleiotropic genetic variants to estimate causal effects. Am. J. Epidemiol 181 (4), 251–260. [PubMed: 25632051]

Busatto GF, Garrido GEJ, Almeida OP, Castro CC, Camargo CHP, Cid CG, Buchpiguel CA, Furuie S, Bottino CM, 2003 A voxel-based morphometry study of temporal lobe gray matter reductions in alzheimer's disease. Neurobiol. Aging 24 (2), 221–231. [PubMed: 12498956]

Cimino CR, Verfaellie M, Bowers D, Heilman K, 1991 Autobiographical memory - influence of right-hemisphere damage on emotionality and specificity. Brain Cogn. 15 (1), 106–118. [PubMed: 2009169]

Consortium TGP, 2010 A map of human genome variation from population-scale sequencing. Nature 467 (7319), 1061. [PubMed: 20981092]

Convit A, De Leon MJ, Tarshish C, De Santi S, Tsui W, Rusinek H, George A, 1997 Specific hippocampal volume reductions in individuals at risk for alzheimer's disease. Neurobiol. Aging 18 (2), 131–138. [PubMed: 9258889]

Davey Smith G, Ebrahim S, 2008 Mendelian Randomization: Genetic Variants as Instruments for Strengthening Causal Inference in Observational Studies. In: Biosocial Surveys. National Academies Press, pp. 336–366.

DelGreco F, Minelli C, Sheehan NA, Thompson JR, 2015 Detecting pleiotropy in mendelian randomisation studies with summary data and a continuous outcome. Stat. Med 34 (21), 2926–2940. [PubMed: 25950993]

Demey I, Ventrice F, Rojas G, Somale V, Zubiri V, 2015 Alzheimer'S disease dementia involves the corpus callosum and the cingulum: a diffusion tensor imaging study. Alzheimer's and Dementia: The Journal of the Alzheimer's Association 11 (7), P409–P410.

Deng Y, Pan W, 2017 Conditional analysis of multiple quantitative traits based on marginal GWAS summary statistics. Genet. Epidemiol 41 (5), 427–436. [PubMed: 28464407]

Deng Y, Pan W, 2017 Testing genetic pleiotropy with GWAS summary statistics for marginal and conditional analyses. Genetics 207 (4), 1285–1299. [PubMed: 28971959]

Deng Y, Pan W, 2018 Improved use of small reference panels for conditional and joint analysis with GWAS summary statistics. Genetics 209 (2), 401–408. [PubMed: 29674520]

Eleanor Sanderson FW, Davey Smith G, Borden J, 2019 An examination of multivariable mendelian randomization in the single-sample and two sample summary data settings. Int. J. Epidemiol 48 (3), 713–727. [PubMed: 30535378]

Elliott LT, et al., 2018 Genome-wide association studies of brain imaging phenotypes in UK biobank. Nature 562 (7726), 210–216. [PubMed: 30305740]

Fathy YY, Hoogers SE, Berendse HW, van der Werf YD, Visser PJ, de Jong FJ, van de Berg WDJ, 2019 Differential insular cortex sub-regional atrophy in neurodegenerative diseases: a systematic review and meta-analysis. Brain Imaging Behav.

Fox N, et al., 1996 Presymptomatic hippocampal atrophy in alzheimer's disease - a longitudinal MRI study. Brain 119, 2001–2007. [PubMed: 9010004]

Frozza R, Lourenco M, De Felice F, 2018 Challenges for alzheimer's disease therapy: insights from novel mechanisms beyond memory defects. Front. Neurosci 12.

Galton JC, et al., 2001 Differing patterns of temporal atrophy in alzheimers disease and semantic dementia. Neurology 57 (2), 216–225. [PubMed: 11468305]

Gamazon ER, Wheeler HE, Shah KP, Mozaffari SV, Aquino-Michaels K, Car-roll RJ, Eyler AE, Denny JC, Nicolae DL, Cox NJ, Im HK, 2015 A gene-based association method for mapping traits using reference transcriptome data. Nat. Genet 47 (9).

Gusev A, et al., 2016 Integrative approaches for large-scale transcriptome-wide association studies. Nat. Genet 48 (3), 245–255. [PubMed: 26854917]

Haghshomar M, Dolatshahi M, Sherbaf F, Moghaddam H, Shandiz MS, Aarabi M, 2018 Disruption of inferior longitudinal fasciculus microstructure in parkinson's disease: a systematic review of diffusion tensor imaging studies. Front. Neurol 9.

Hemani G, Bowden J, Davey Smith G, 2018 Evaluating the potential role of pleiotropy in mendelian randomization studies. Hum. Mol. Genet 27 (R2), R195–R208. [PubMed: 29771313]

Herold C, Hooli BV, Mullin K, Liu T, Roehr JT, Mattheisen M, Parrado AR, Bertram L, Lange C, Tanzi RE, 2016 Family-based association analyses of imputed genotypes reveal genome-wide significant association of alzheimer's disease with OSBPL6, PTPRG and PDCL3. Mol. Psychiatry 21 (11).

Hibar DP, et al., 2015 Common genetic variants influence human subcortical brain structures. Nature 520 (7546).

Hondius DC, Eigenhuis KN, Morrema THJ, van der Schors RC, van Nierop P, Bugiani M, Li KW, Hoozemans JJM, Smit AB, Rozemuller AJM, 2018 Proteomics analysis identifies new markers associated with capillary cerebral amyloid angiopathy in alzheimer's disease. Acta Neuropathologica Communinications 6 (1). urn:issn:2051-5960

Jiji S, Smitha KA, Gupta AK, Pillai VPM, Jayasree RS, 2013 Segmentation and volumetric analysis of the caudate nucleus in alzheimer's disease. Eur. J. Radiol 82 (9), 1525–1530. [PubMed: 23664648]

Johnston KM, Gustafson P, Levy AR, Grootendorst P, 2008 Use of instrumental variables in the analysis of generalized linear models in the presence of unmeasured confounding with applications to epidemiological research. Stat. Med 27 (9), 1539–1556. [PubMed: 17847052]

de Jong LW, van der Hiele K, Veer IM, Houwing JJ, Westendorp RGJ, Bollen ELEM, de Bruin PW, Middelkoop HAM, van Buchem MA, van der Grond J, 2008 Strongly reduced volumes of putamen and thalamus in alzheimer's disease: an MRI study. Brain 131 (12), 3277–3285. [PubMed: 19022861]

Kim J, Zhang Y, Pan W, 2016 Powerful and adaptive testing for multi-trait and multi-SNP associations with GWAS and sequencing data. Genetic Epidemiology 40 (7). 646–646

Knutson KA, Pan W, 2020 Integrating brain imaging endophenotypes with GWAS for alzheimer's disease. Quant. Biol. TBD (TBD), TBD

Ko AM-S, Tu H-P, Liu T-T, Chang J-G, Yuo C-Y, Chiang S-L, Chang S-J, Liu Y-F, Ko AM-J, Lee C-H, Lee C-P, Chang C-M, Tsai S-F, Ko Y-C, 2013 Alpk1 genetic regulation and risk in relation to gout. Int. J. Epidemiol 42 (2), 466. [PubMed: 23569188]

Labrecque J, Swanson S, 2018 Understanding the assumptions underlying instrumental variable analyses: a brief review of falsification strategies and related tools. Curr. Epidemiol. Rep 5 (3), 214–220. [PubMed: 30148040]

Lambert J-C, et al., 2013 Meta-analysis of 74,046 individuals identifies 11 new susceptibility loci for alzheimer's disease. Nat. Genet 45, 1452–1458. [PubMed: 24162737]

Larsson S, Markus H, 2017 Branched-chain amino acids and alzheimer's disease: a mendelian randomization analysis. Sci. Rep 7 (1). 13604–13604 [PubMed: 29051501]

Launer JL, White RL, Petrovitch WH, Ross DG, Curb DJ, 2001 Cholesterol and neuropathologic markers of AD: apopulation-based autopsy study. Neurology 57 (8), 1447–1452. [PubMed: 11673587]

Lin W, Feng R, Li H, 2015. Regularization methods for high-dimensional instrumental variables regression with an application to genetical genomics. Journal of the American Statistical

Association 110 (509), 270–288. http://www.tandfonline.com/doi/abs/10.1080/01621459.2014.908125 [PubMed: 26392642]

Lindberg O, Walterfang M, Looi JCL, Malykhin N, Ostberg P, Zandbelt B, Styner M, Paniagua B, Velakoulis D, Orndahl E, Wahlund L-O, 2012 Hippocampal shape analysis in alzheimer's disease and frontotemporal lobar degeneration subtypes. J. Alzheimers Dis 30 (2), 355. [PubMed: 22414571]

Mak TSH, et al., 2017 Polygenic scores via penalized regression on summary statistics. Genet. Epidemiol 41 (6), 469–480. [PubMed: 28480976]

Manichaikul A, Mychaleckyj J, Rich S, Daly K, Sale M, Chen W-M, 2010 Robust relationship inference in genome-wide association studies. Bioinformatics 26 (22), 2867–2873. http://search.proquest.com/docview/849436321/ [PubMed: 20926424]

Markowitsch HJ, Thiel A, Reinkemeier M, Kessler J, Koyuncu A, Heiss W-D, 2000 Right amygdalar and temporofrontal activation during autobiographic, but not during fictitious memory retrieval. Behav. Neurol 12 (4), 181. [PubMed: 11568430]

Matsuda H, 2017 Neuroimaging diagnosis for Alzheimer's disease and other dementias. Springer, Tokyo, Japan.

Mayo CD, Garcia-Barrera MA, Mazerolle EL, Ritchie LJ, Fisk JD, Gawryluk JR, 2019 Relationship between DTI metrics and cognitive function in alzheimer's disease. Front Aging Neurosci 10.

Newey WK, 2013 Nonparametric instrumental variables estimation. American Economic Review 103 (3), 550–556.

Pacini D, Windmeijer F, 2016 Robust inference for the two-sample 2SLS estimator. Econ. Lett 146, 50–54. [PubMed: 27667880]

Pan W, 2009 Asymptotic tests of association with multiple SNPs in linkage disequilibrium. Genet. Epidemiol 33 (6), 497–507. [PubMed: 19170135]

Pan W, Kwak I-Y, Wei P, 2015 A powerful pathway-based adaptive test for genetic association with common or rare variants. The American Journal of Human Genetics 97 (1), 86–98. [PubMed: 26119817]

Pattee J, Pan W, 2020 Penalized regression and model selection methods for polygenic scores on GWAS summary statistics. Manuscript.

Philippi N, Botzung A, Noblet V, Rousseau F, Despres O, Cretin B, Kremer S, Blanc F, Manning L, 2015 Impaired emotional autobiographical memory associated with right amygdalar-hippocampal atrophy in alzheimer's disease patients. Front. Aging Neurosci 7.

Pickrell JK, 2015 Fulfilling the promise of mendelian randomization. bioRxiv doi: 10.1101/018150.

Pini L, Pievani M, Bocchetta M, Altomare D, Bosco P, Cavedo E, Galluzzi S, Marizzoni M, Frisoni GB, 2016 Brain atrophy in alzheimer's disease and aging. Ageing Res. Rev 30, 25. [PubMed: 26827786]

Pluta D, Ombao H, Chen C, Xue G, Moyzis R, Yu Z, 2017 Adaptive mantel test for association testing in imaging genetics data. arXiv.

Pluta D, Yu Z, Shen T, Chen C, Xue G, Ombao H, 2018 Statistical methods and challenges in connectome genetics. Statistics and Probability Letters 136, 83–86.

Potkin SG, Guffanti G, Lakatos A, Turner JA, Kruggel F, Fallon JH, Saykin AJ, Orro A, Lupoli S, Salvi E, Weiner M, Macciardi F, 2009 Hippocampal atrophy as a quantitative trait in a genome-wide association study identifying novel susceptibility genes for alzheimer's disease (imaging genetics in AD). PLoS ONE 4 (8), e6501.

Poulin SP, Dautoff R, Morris JC, Barrett LF, Dickerson BC, 2011 Amygdala atrophy is prominent in early alzheimer's disease and relates to symptom severity. Psychiatry Research: Neuroimaging 194 (1), 7–13. [PubMed: 21920712]

Rees JMB, Wood AM, Burgess S, 2017 Extending the MR-egger method for multivariable mendelian randomization to correct for both measured and unmeasured pleiotropy. Stat. Med 36 (29), 4705. [PubMed: 28960498]

Ryzhakov G, West N, Franchini F, Simon C, Ilott N, Sansom S, Bullers S, Pearson C, Costain A, Vaughan-Jackson A, Goettel J, Ermann J, Horwitz B, Buti L, Lu X, Mukhopadhyay S, Snapper S, Powrie F, 2018 Alpha kinase 1 controls intestinal inflammation by suppressing the IL-12/th1 axis. Nature Communications 9 (1), 1–13. http://search.proquest.com/docview/2108834110/

Sarica A, Vasta R, Novellino F, Vaccaro MG, Cerasa A, Quattrone A, Initiative TADN, 2018 Mri asymmetry index of hippocampal subfields increases through the continuum from the mild cognitive impairment to the alzheimer's disease.(report). Front. Neurosci 12.

Saykin AJ, et al., 2015 Genetic studies of quantitative MCI and AD phenotypes in ADNI: progress, opportunities, and plans. Alzheimers and Dementia 11 (7), 792–814.

Schaid DJ, et al., 2016 Statistical methods for testing genetic pleiotropy. Genetics 204, 483–497. [PubMed: 27527515]

Shahapal A, Cho EB, Yong HJ, Jeong I, Kwak H, Lee JK, Kim W, Kim B, Park H-C, Lee WS, Kim H, Hwang J-I, Seong JY, 2019 Fam19a5 expression during embryogenesis and in the adult traumatic brain of knock-in mice. Front. Neurosci 13, 917. [PubMed: 31543758]

Shen L, Thompson P, Potkin S, Bertram L, Farrer L, Foroud T, Green R, Hu X, Huentelman M, Kim S, Kauwe J, Li Q, Liu E, Macciardi F, Moore J, Munsie L, Nho K, Ramanan V, Risacher S, Stone D, Swaminathan S, Toga A, Weiner M, Saykin A, 2014 Genetic analysis of quantitative phenotypes in AD and MCI: imaging, cognition and biomarkers. Brain Imaging Behav. 8 (2), 183–207. [PubMed: 24092460]

Shen L, Thompson PM, 2020 Brain imaging genomics: integrated analysis and machine learning. Proc. IEEE 108 (1), 125–162.

Silbert LC, Quinn JF, Moore MM, Corbridge E, Ball MJ, Murdoch G, Sexton G, Kaye JA, 2003 Changes in premorbid brain volume predict alzheimers disease pathology. Neurology 61 (4), 487–492. [PubMed: 12939422]

, 2005 In: Taudes A (Ed.), Adaptive information systems and modeling in economics and management science. Springer, Wien ; New York.

Toniolo S, Serra L, Olivito G, Cercignani M, Bozzali M, 2018 Cerebellar white matter disruption in AD patients: a diffusion tensor imaging study. European Journal Of Neurology 25 (s2). 93–93

Trushina E, Dutta T, Persson X-M, Mielke M, Petersen R, 2013 Identification of altered metabolic pathways in plasma and CSF in mild cognitive impairment and alzheimer's disease using metabolomics. PLoS One 8 (5), e63644. http://search.proquest.com/docview/1353319300/

Uddin MJ, et al., 2015 Instrumental variable analysis in epidemiologic studies: an overview of the estimation methods. Pharm. Anal. Acta 6 (4).

Verbanck M, Chen C-Y, Neale B, Do R, 2018 Detection of widespread horizontal pleiotropy in causal relationships inferred from mendelian randomization between complex traits and diseases. Nat. Genet 50 (5), 693. [PubMed: 29686387]

Wainberg M, et al., 2019 Opportunities and challenges for transcriptome-wide association studies. Nat. Genet 51, 592–599. [PubMed: 30926968]

Walsh M, Montojo C, Sheu Y, Marchette S, Harrison D, Newsome S, Zhou F, Shelton A, Courtney S, 2011 Object working memory performance depends on microstructure of the frontal-occipital fasciculus. Brain Connect. 1 (4).

Wenk G, 2003 Neuropathologic changes in alzheimer's disease. Journal Of Clinical Psychiatry 64, 7–10.

Whitwell JL, Avula R, Senjem ML, Kantarci K, Weigand SD, Samikoglu A, Edmonson HA, Vemuri P, Knopman DS, Boeve BF, Petersen RC, Josephs KA, Jack CR, 2010 Gray and white matter water diffusion in the syndromic variants of frontotemporal dementia. Neurology 74 (16), 1279–1287. [PubMed: 20404309]

Williams LB, Javed A, Sabri A, Morgan DJ, Huff CD, Grigg JR, Heng XT, Khng AJ, Hollink IHIM, Morrison MA, Owen LA, Anderson K, Kinard K, Greenlees R, Novacic D, Nida Sen H, Zein WM, Rodgers GM, Vitale AT, Haider NB, Hillmer AM, Ng PC, Shankaracharya A, Cheng L, Zheng MC, Gillies M, van Slegtenhorst PM, van Hagen TOAR, Missotten GL, Farley M, Polo J, Malatack J, Curtin F, Martin S, Arbuckle SI, Alexander M, Chircop S, Davila KB, Digre RV, Jamieson MM, Deangelis MM, 2019 Alpk1 missense pathogenic variant in five families leads to rosah syndrome, an ocular multisystem autosomal dominant disorder. Genet. Med 21 (9), 2103. [PubMed: 30967659]

Wu C, 2020 Multi-trait genome-wide analyses of the brain imaging phenotypes in UK biobank. Genetics 215 (4), 947–958. [PubMed: 32540950]

Wu Y, Sun D, Wang Y, Wang Y, Ou S, 2016 Segmentation of the cingulum bundle in the human brain: a new perspective based on DSI tractography and fiber dissection study.(report)(author abstract). Front. Neuroanat 10.

Xu Z, Wu C, Pan W, 2017 Imaging-wide association study: integrating imaging endophenotypes in GWAS. Neuroimage 159, 159–169. [PubMed: 28736311]

Xue H, Pan W, 2019 Some statistical consideration in transcriptome-wide association studies. Genet. Epidemiol

Yang J, et al., 2012 Conditional and joint multiple-SNP analysis of GWAS summary statistics identifies additional variants influencing complex traits. Nat. Genet 44 (4), 369–S3. [PubMed: 22426310]

Yin R-H, Tan L, Liu Y, Wang W-Y, Wang H-F, Jiang T, Radua J, Zhang Y, Gao J, Canu E, Migliaccio R, Filippi M, Gorno-Tempini ML, Yu JT, 2015 Multimodal voxel-based meta-analysis of white matter abnormalities in alzheimer's 13422disease. J. Alzheimers Dis 47 (2), 495–507. [PubMed: 26401571]

Zhang L, Guo XQ, Chu JF, Zhang X, Yan ZR, Li YZ, 2015 Potential hippocampal genes and pathways involved in alzheimer's disease: a bioinformatic analysis. Genet. Mol. Res 14 (2), 7218. [PubMed: 26125932]

Zhang HY, Schuff TN, Jahng HG, Bayne JW, Mori LS, Schad WL, Mueller WS, Du WA, Kramer WJ, Yaffe WK, Chui WH, Jagust WW, Miller WB, Weiner WM, 2007 Diffusion tensor imaging of cingulum fibers in mild cognitive impairment and alzheimer's disease. Neurology 68 (1), 13–19. [PubMed: 17200485]

Zhao B, Luo T, Li T, Li Y, Zhang J, Shan Y, Wang X, Yang L, Zhou F, Zhu Z, Zhu H, 2019 Genome-wide association analysis of 19,629 individuals identifies variants influencing regional brain volumes and refines their genetic co-architecture with cognitive and mental health traits. Nat. Genet 51 (11), 1637. [PubMed: 31676860]

Zhao B, Shan Y, Yang Y, Li T, Luo T, Zhu Z, Li Y, Zhu H, 2019 Transcriptome-wide association analysis of 211 neuroimaging traits identifies new genes for brain structures and yields insights into the gene-level pleiotropy with other complex traits. bioRxiv doi: 10.1101/842872.

Zhao L, Tang Y, Tan J, Wang J, Chen G, Zhu B, 2018 The effect of NR4a1 on APP metabolism and tau phosphorylation. Genes and Diseases 5 (4), 342–348. [PubMed: 30591936]

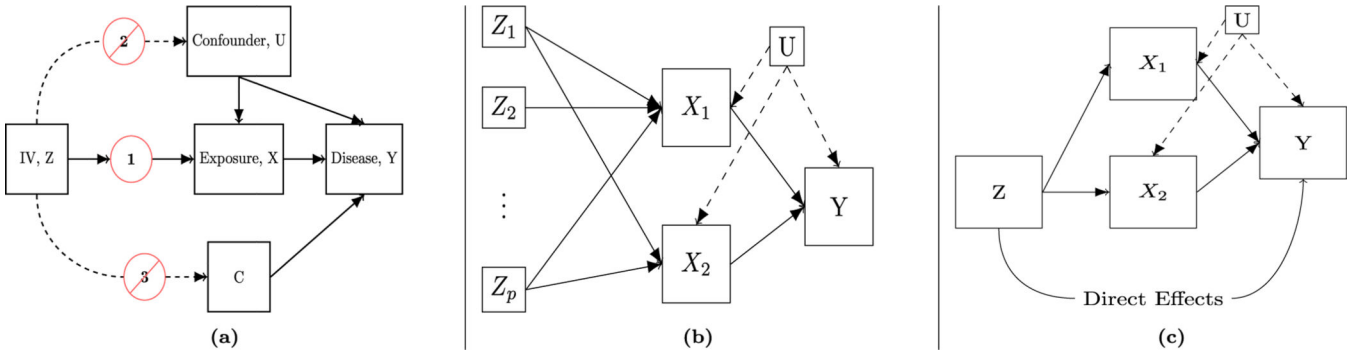


**Fig. 1.**

a) A causal directed acyclic graph (DAG) representing the assumed model for univariate IV analysis with satisfaction of all 3 instrumental variable assumptions: **1) Relevance:** Z is correlated with X, **2) Exchangability:** Z is uncorrelated with confounders, and **3) Exclusion Restriction:** Z does not affect Y, except through X. Here, C represents the set of additional causal phenotypes for disease which are not associated with the IVs. b) The assumed model under the MV-IWAS framework, allowing the IVs to be pleiotropic for multiple causal phenotypes ($X_1$ and $X_2$) for Y. Here, $Z_1$ and $Z_p$ exhibit horizontal pleiotropy, while $Z_2$ does not. Under this setting, UV-IWAS estimates for $X_1$ or $X_2$ will be inconsistent. c) The assumed model for MV-IWAS-Egger, where SNPs Z are pleiotropic for pathways outside of $X_1$ and $X_2$, as represented by the direct pathway from Z to Y.

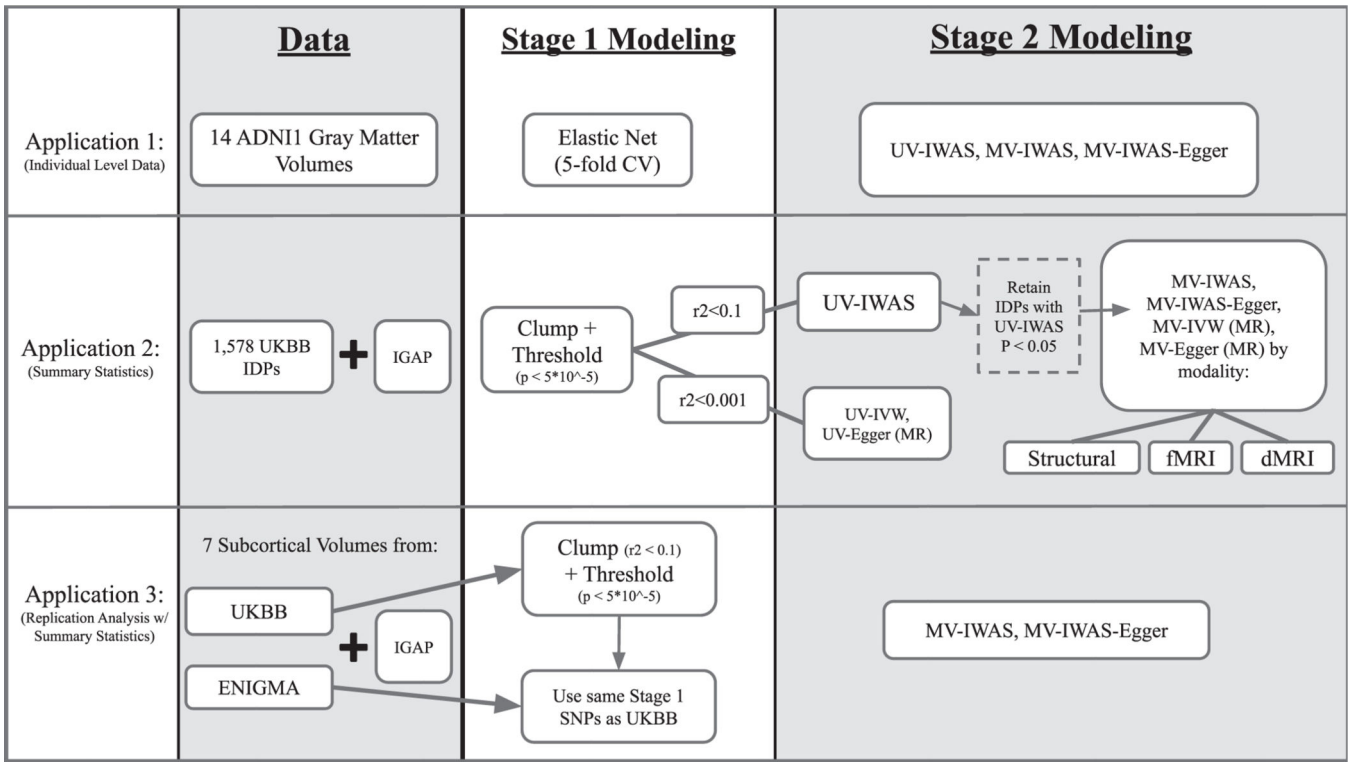


**Fig. 2.**
Workflow for applied analysis of 3 different data sources.

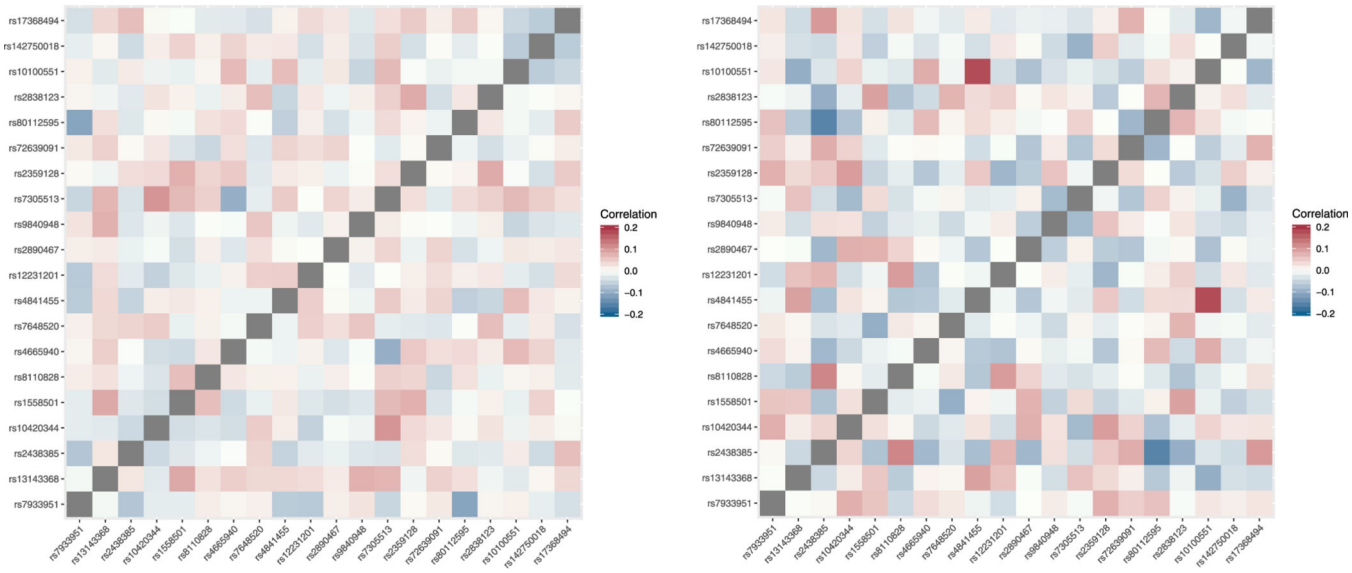


(a) LD Correlations for the 20 simulated SNPs, estimated using ADNI1 data.

(b) LD Correlations for the 20 simulated SNPs, estimated using 1000G data.

**Fig. 3.**

(a)LD Correlations for the 20 simulated SNPs, estimated using ADNI1 data. (b)LD Correlations for the 20 simulated SNPs, estimated using 1000G data.

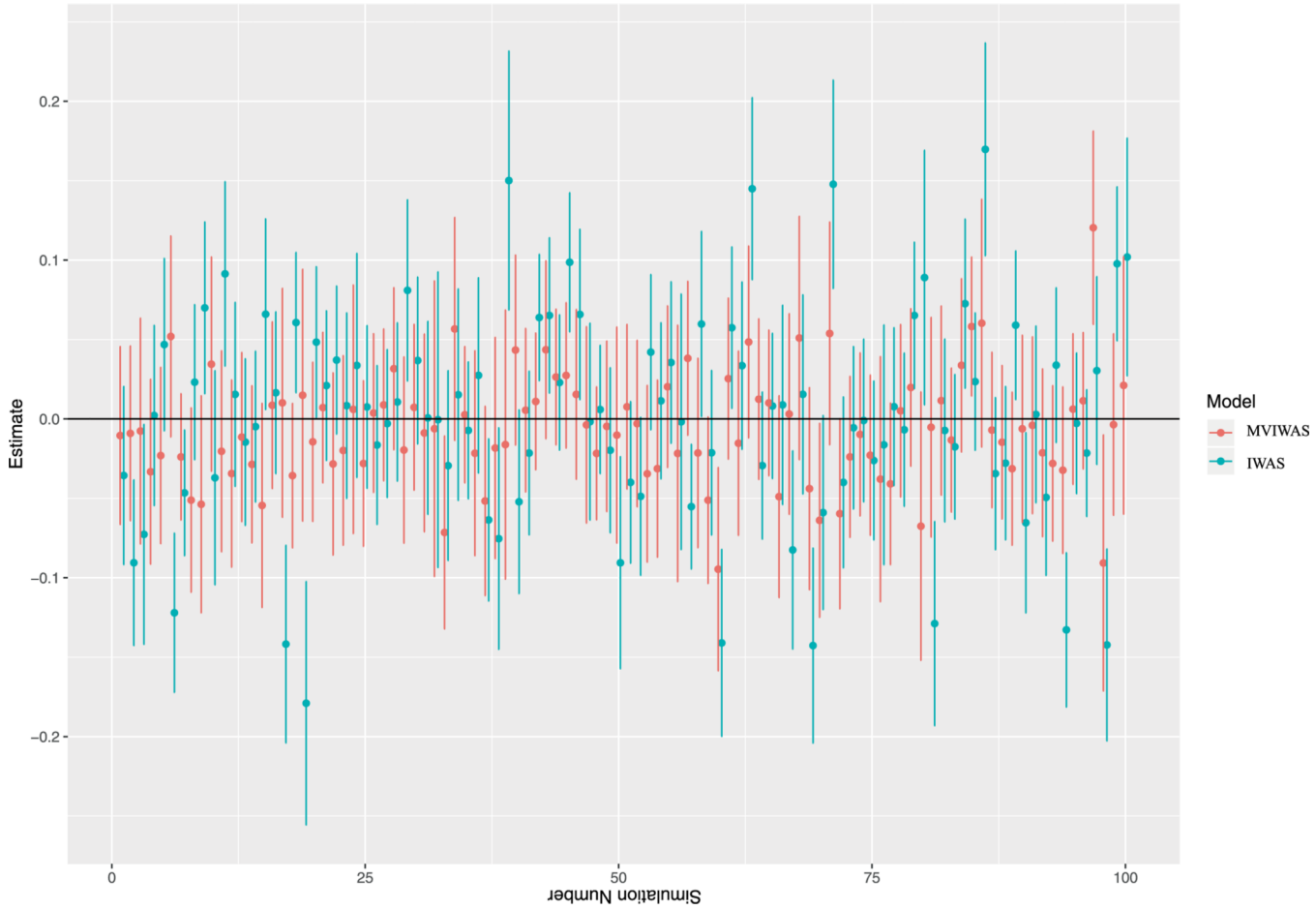


**Fig. 4.**

95% confidence intervals for $\beta_1$ from the first 100 iterations from the 2 sample simulations for a quantitative disease trait. The true value for $\beta_1 = 0$.

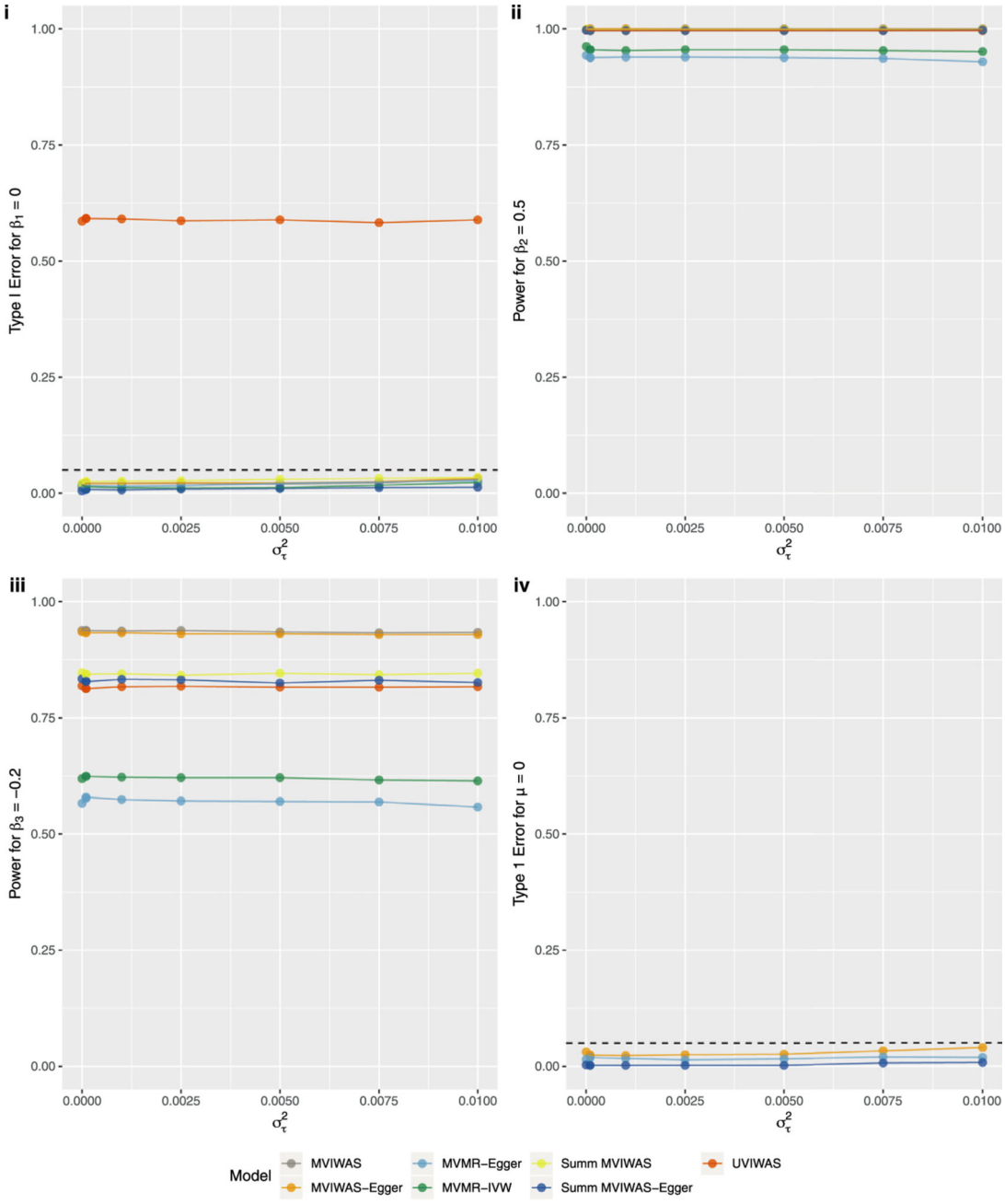


(a) $\mu = 0$

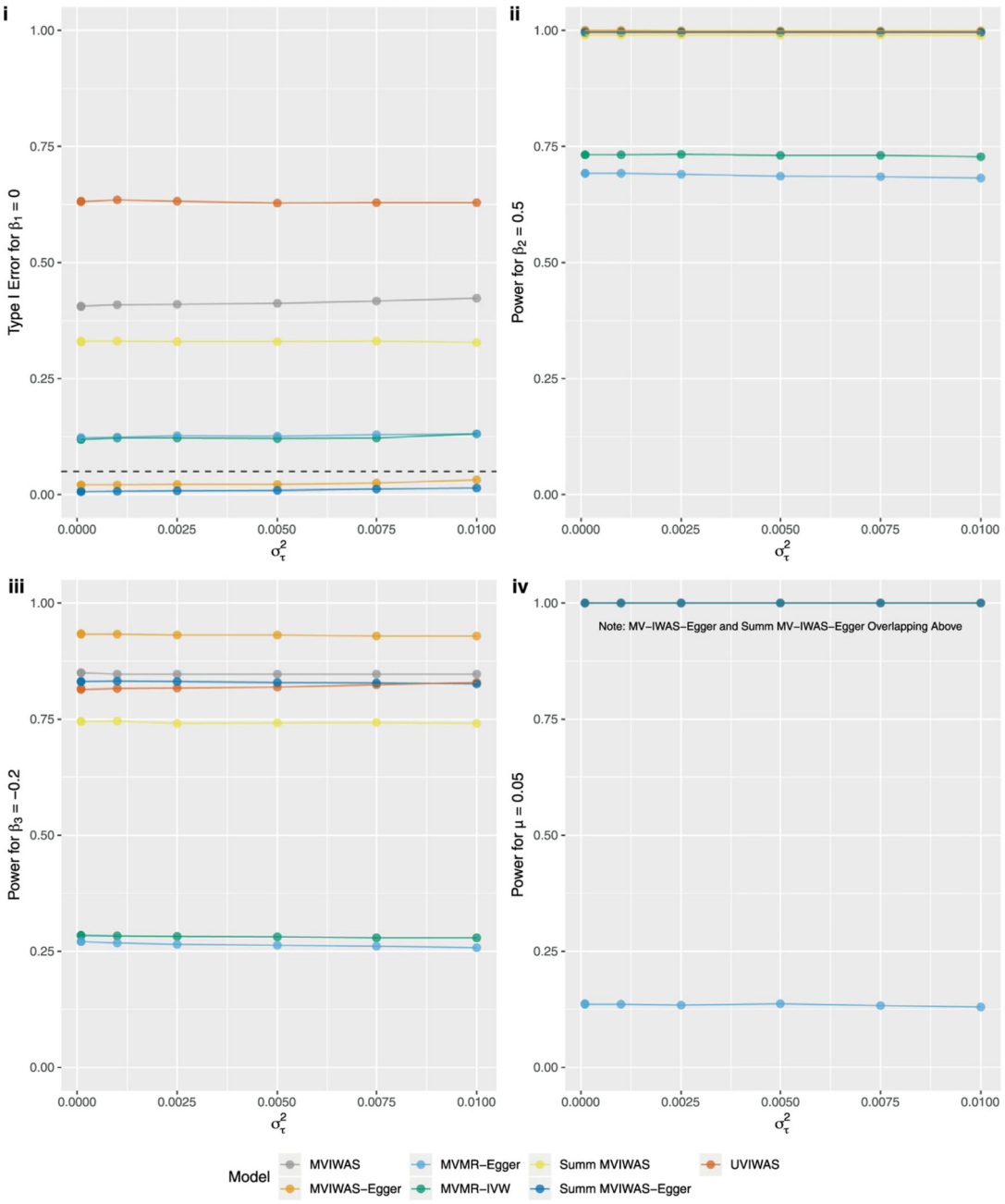


(b) $\mu = 0{:}05$

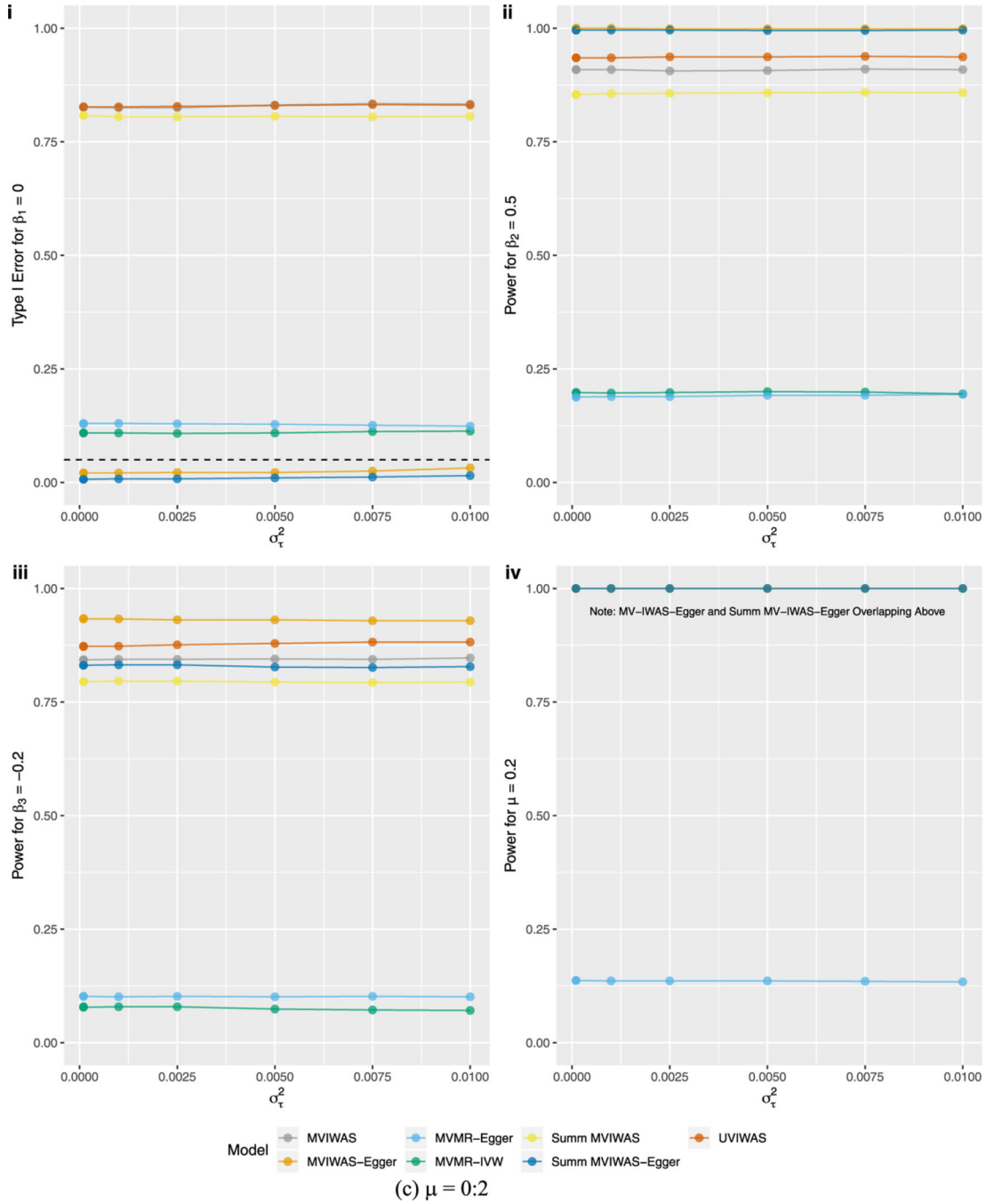


**Fig. 5.**

Simulation Type I Error and Power across different magnitudes of $\sigma_\tau^2$ and $\mu$. For each setting of $\mu$: i) Type I error for $\beta_1$ ii) Power for $\beta_2$ iii) Power for $\beta_3$ iv) Power/Type I Error for $\mu$. LD estimated using 1000 Genomes for all Summary Statistic IWAS methods (Summ MVI-WAS and Summ MVIWAS-Egger).

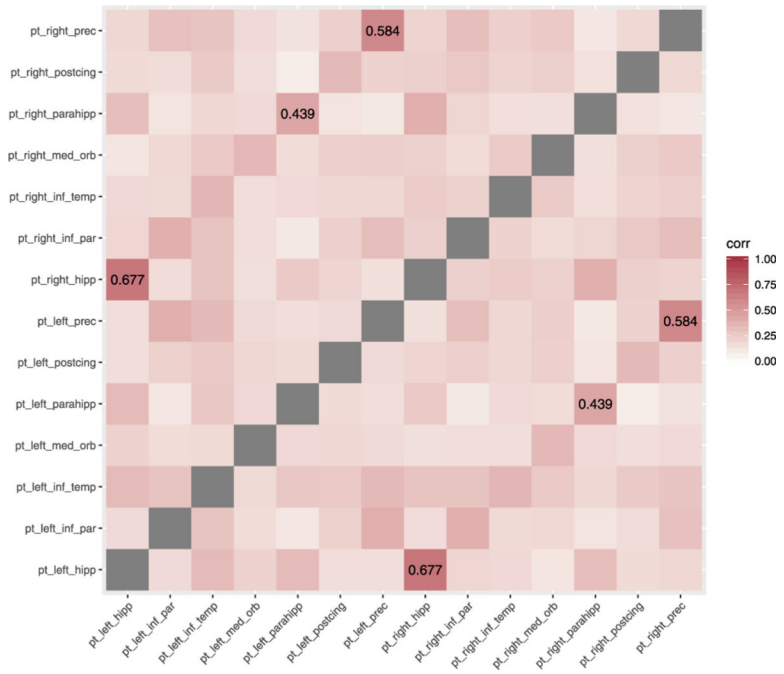


**Fig. 6.**
Correlations between the 14 Imputed ADNI1 Endophenotypes.

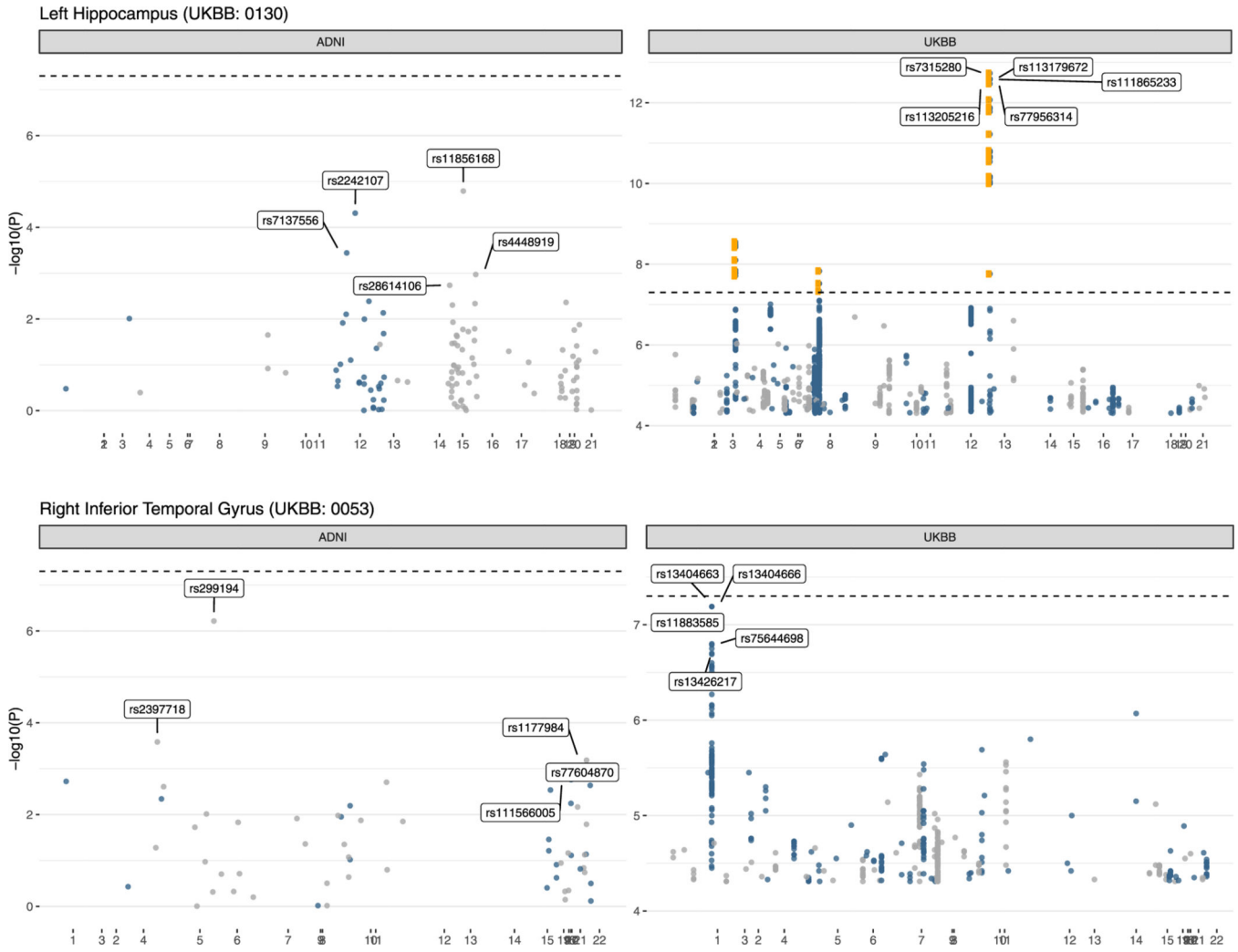


**Fig. 7.**

Manhattan Plots reflecting Stage 1 Models for the 2 ADNI (left) Endophenotypes significant for MV-IWAS with comparison to comparable UKBB T1 FAST (right) IDPs. Note the difference of y-axis scale for the ADNI and UKBB plots; the notably higher peaks for the UKBB marginal p-values can be explained by the substantial difference in sample size between the two studies. We further note that UKBB IDP 0053 is a measure of only the anterior division of the left inferior temporal gyrus and is thereby not *directly* comparable to the corresponding ADNI measure.

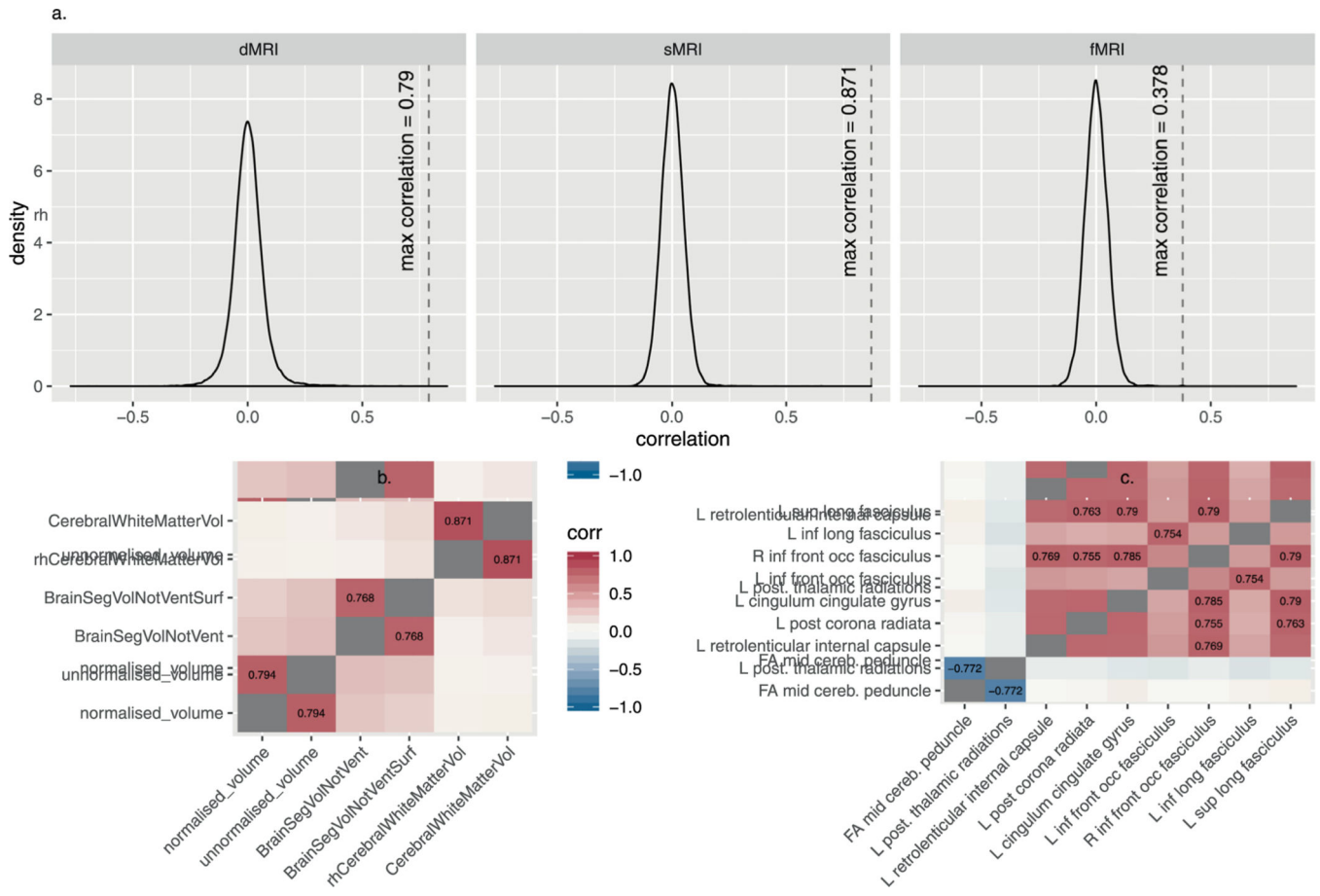


**Fig. 8.**

a) Distribution of pairwise pearson correlations for IDPs with unadjusted UV-IWAS p-values below 0.05 by modality. This includes 306 dMRI, 279 sMRI and 146 fMRI imputed IDPs. b) 3 IDP pairs of sMRI IDPs with correlations > 0.75. c) 7 pairwise correlations > 0.75 between imputed dMRI IDPs.

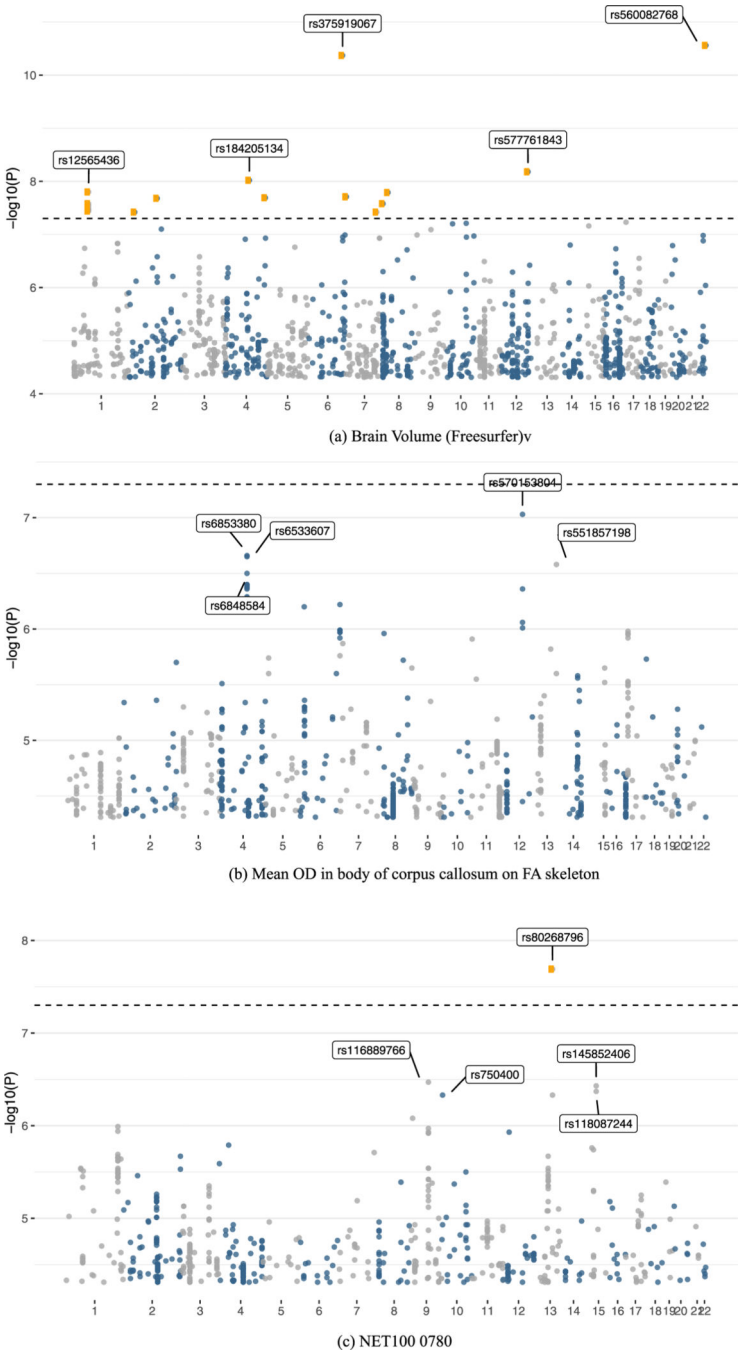


**Fig. 9.**

Manhattan Plots for Stage 1 SNPs used for each of the IDPs with the greater causal effect estimate for MV-IWAS-Egger.

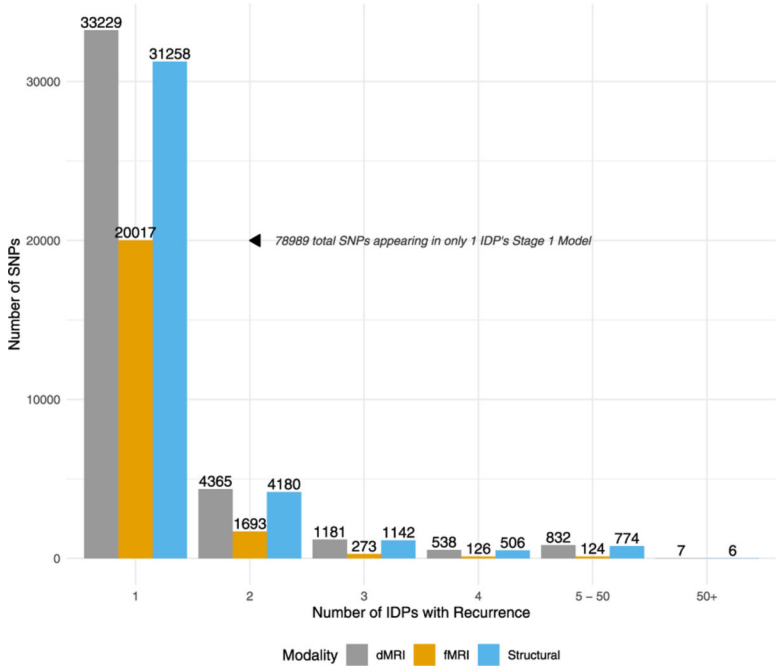


**Fig. 10.**

Number of SNPs which are included in 1, 2, 3, 4, 5–50, or 50+ UK Biobank IDP's Stage 1 IWAS model by modality. Recurrence in more than one Stage 1 IDP model gives evidence for possible pleiotropic effects that will cause inconsistency in the univariate IWAS approach.

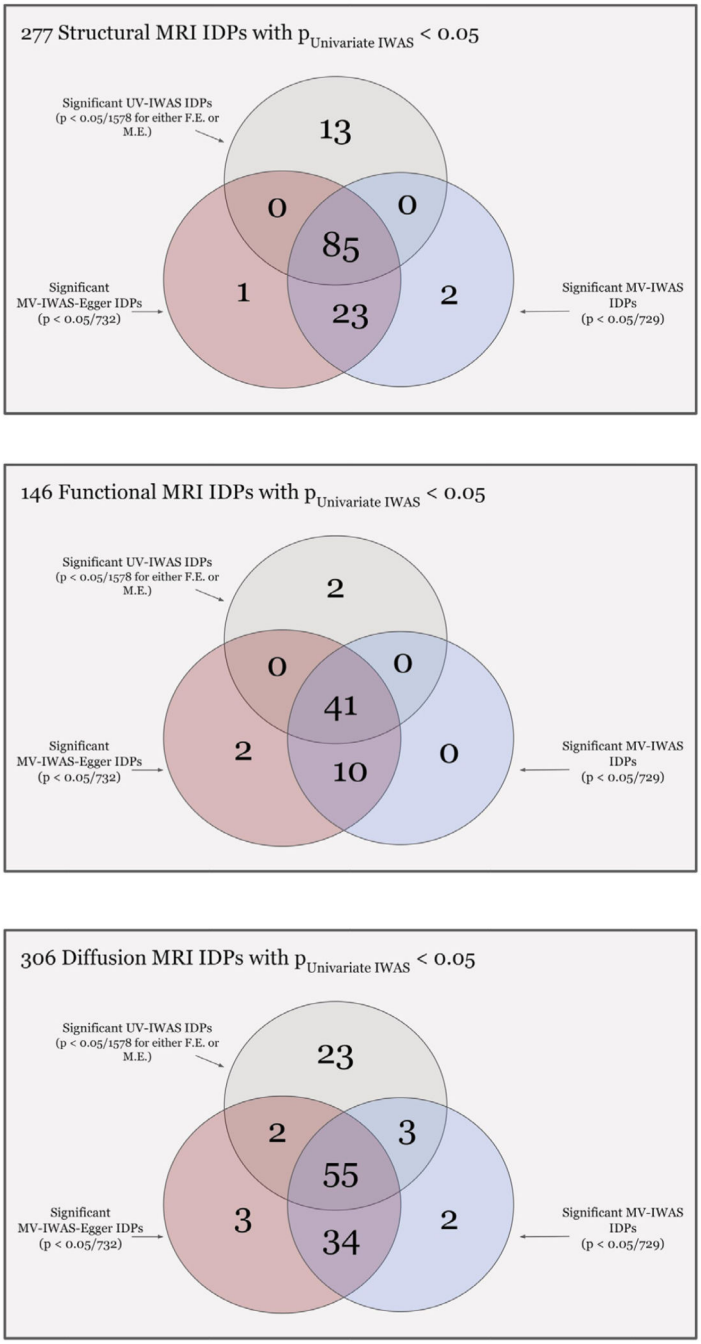


**Fig. 11.**

Comparison of the significant phenotypes identified by the univariate and multivariate IWAS tests for Structural, Diffusion, and Functional MRI IDPs. The quantities given within the red, blue, and grey circles indicate the number of IDPs which were significant for MV-IWAS-Egger, MV-IWAS, and UV-IWAS, respectively. Their intersection reflects IDPs which were significant under all 3 tests.

**Table 1**

Number of genome-wide SNPs with non-zero elastic net coefficients used as Stage 1 SNPs for 14 ADNI1 endophenotypes. Elastic net was fit with confounder adjusted residuals as a response and genotype matrix as predictors.

| Endophenotype | Number of Stage 1 SNPs (Left/Right) |
|---|---|
| Hippocampus | 148/101 |
| Inferior Parietal | 80/77 |
| Inferior Temporal | 310/77 |
| Medial Orbitofrontal | 69/1126 |
| Parahippocampus | 84/183 |
| Precuneus | 234/175 |
| Posterior Cingulate | 221/337 |

**Table 2**

Mean Simulation Estimates, Power, and 95% Coverages for 1- and 2- sample univariate versus multivariate IWAS for quantitative and binary disease traits with 3 simulated endophenotypes using p = 20 randomly selected genome-wide SNPs. True values for the quantitative and binary traits are $\beta = (0, 0.5, -0.2)$ and $\beta = (0, 0.08, -0.08)$, respectively. 30% of SNPs are invalid IVs. Power estimates (or alternatively 1 – 95% Coverage) for $\beta_1 = 0$ correspond to the Type I Error rate.

| | | | |
|---|---|---|---|
| 2-Sample Test with Quantitative Disease Trait, True $\beta = (0, 0.5, -0.2)$ | | | |
| | $\hat{\beta}_1(SE), \hat{\beta}_2(SE), \hat{\beta}_3(SE)$ | 95% Simulation Coverages | Power |
| Univariate IWAS (Individual Level Data) | −0.0005 (0.027), 0.479 (0.056), −0.177 (0.055) | 0.541, 0.676, 0.363 | 0.459, 0.990, 0.739 |
| MV-IWAS (Individual Level Data) | −0.003 (0.029), 0.491 (0.065), −0.208 (0.064) | 0.949, 0.946, 0.939 | 0.051, 0.992, 0.861 |
| MV-IWAS (1000G) | −0.002 (0.041), 0.495 (0.092), −0.208 (0.091) | 0.982, 0.970, 0.983 | 0.018, 0.983, 0.682 |
| 2-Sample Test with Binary Disease Trait, True $\beta = (0, 0.08, -0.08)$ | | | |
| | $\hat{\beta}_1(SE), \hat{\beta}_2(SE), \hat{\beta}_3(SE)$ | 95% Simulation Coverages | Power |
| Univariate IWAS (Individual Level Data) | 0 (0.007), 0.074 (0.014), −0.074 (0.014) | 0.654, 0.525, 0.506 | 0.346, 0.886, 0.901 |
| MV-IWAS (Individual Level Data) | 0 (0.007), 0.077 (0.017), −0.077 (0.017) | 0.951, 0.936, 0.948 | 0.049, 0.962, 0.961 |
| MV-IWAS (1000G) | 0 (0.010), 0.077 (0.023), −0.077 (0.023) | 0.991, 0.99, 0.989 | 0.009, 0.891, 0.918 |
| 1-Sample Test with Quantitative Disease Trait, True $\beta = (0, 0.5, -0.2)$ | | | |
| | $\hat{\beta}_1(SE), \hat{\beta}_2(SE), \hat{\beta}_3(SE)$ | 95% Simulation Coverages | |
| Univariate IWAS (Individual Level Data) | 0.002 (0.019), 0.515 (0.039), −0.186 (0.039) | 0.441, 0.581, 0.251 | 0.559, 0.997, 0.809 |
| MV-IWAS (Individual Level Data) | 0.002 (0.02), 0.515 (0.046), −0.186 (0.046) | 0.985, 0.971, 0.966 | 0.015, 1, 0.932 |
| MV-IWAS (1000G) | 0.003 (0.029), 0.520 (0.065), −0.187 (0.065) | 0.974, 0.946, 0.958 | 0.026, 1, 0.817 |
| 1-Sample Test with Binary Disease Trait, True $\beta = (0, 0.08, -0.08)$ | | | |
| | $\hat{\beta}_1(SE), \hat{\beta}_2(SE), \hat{\beta}_3(SE)$ | 95% Simulation Coverages | Power |
| Univariate IWAS (Individual Level Data) | 0 (0.005), 0.077 (0.010), −0.074 (0.010) | 0.508, 0.389, 0.368 | 0.492, 0.941, 0.933 |
| MV-IWAS (Individual Level Data) | 0 (0.005), 0.079 (0.012), −0.075 (0.011) | 0.953, 0.938, 0.923 | 0.049, 0.991, 0.989 |
| MV-IWAS (1000G) | 0 (0.007), 0.079 (0.017), −0.076 (0.016) | 0.985, 0.983, 0.981 | 0.015, 0.976, 0.968 |

**Table 3**

Univariate and multivariate tests of 14 ADNI1 enodphenotypes. Stars indicate significance at a Bonferonni adjusted significant threshold of 0.05/14 for UV- and MV-IWAS and 0.05/15 for MV-IWAS-Egger.

| | | UV-IWAS | | | MV-IWAS MV-IWAS-Egger | | |
|---|---|---|---|---|---|---|---|
| **Volumetric Phenotype (L/R)** | **# of SNPs** | **Estimate** | **SE** | **P** | **Estimate** | **SE** | **P** |
| $\mu$ | | | | | −0.001 | 0.015 | 0.899 |
| Medial Orbitofronal Cortex | 69/126 | −0.045/−0.079 | 0.015/0.015 | 3.77e-03/2.77e-07* | 0.019/−0.034 0.019/−0.034 | 0.015/0.016 0.015/0.016 | 0.205/3.45e-02 0.203/3.44e-02 |
| Posterior Cingulate Cortex | 221/337 | −0.053/−0.061 | 0.015/0.015 | 6.35e-04*/6.77e-05* | 0.009/−0.006 0.009/−0.006 | 0.015/0.015 0.015/0.015 | 0.540/0.679 0.538/0.679 |
| Inferior Temporal Cortex | 310/77 | −0.117/−0.073 | 0.015/0.015 | 2.09e-14*/2.13e-06* | −0.038/−0.007 −0.038/−0.008 | 0.016/0.015 0.017/0.015 | 2.42e-02/0.623 2.41e-02/0.612 |
| Parahippocampus | 84/183 | −0.089/−0.095 | 0.015/0.015 | 6.29e-09*/6.12e-10* | −0.018/−0.027 −0.018/−0.027 | 0.016/0.016 0.016/0.016 | 0.267/9.69e-02 0.265/9.64e-02 |
| Inferior Parietal Cortex | 80/125 | −0.108/−0.080 | 0.015/0.015 | 2.17e-12*/1.93e-07* | −0.060/−0.005 −0.060/−0.005 | 0.016/0.016 0.016/0.016 | 2.30e-04*/0.752 2.45e-04*/0.746 |
| Precuneus | 234/175 | −0.078/−0.081 | 0.015/0.015 | 3.87e-07*/1.54e-07* | −0.002/−0.014 −0.002/−0.014 | 0.018/0.018 0.018/0.018 | 0.902/0.427 0.891/0.431 |
| Hippocampus | 148/101 | −0.148/−0.137 | 0.014/0.014 | 8.12e-23*/1.85e-19* | −0.082/−0.034 −0.082/−0.033 | 0.020/0.020 0.020/0.020 | 5.16e-05*/9.74e-02 6.03e-05*/ 9.89e-02 |

**Table 4**

MV-IWAS tests of 7 endophenotypes based on summary data from the ENIGMA and UKBB studies. Starred p-values indicate significance at a Bonferonni adjusted significant threshold of 0.05/7 = 0.007.

| IDP | P-Value (ukbb, MV-IWAS) | P-Value (enigma, MV-IWAS) | P-Value (ukbb, MV-IWAS-Egger) | P-Value (enigma, MV-IWAS-Egger) |
|---|---|---|---|---|
| ***μ*** | – | – | 7.809e-06* | 1.931e-05* |
| **Nucleus Accumbens** | 0.00259* | 2.739e-05* | 0.00495* | 2.351e-05* |
| **Amygdala** | 0.86961 | 0.65678 | 0.76329 | 0.76232 |
| **Caudate** | 0.43492 | 0.07467 | 0.23074 | 0.12660 |
| **Hippocampus** | 0.00088* | 0.00474* | 0.00127* | 0.01413 |
| **Pallidum** | 0.65615 | 0.06685 | 0.52996 | 0.05024 |
| **Putamen** | 0.14865 | 0.10710 | 0.08172 | 0.08743 |
| **Thalamus** | 0.42606 | 0.32672 | 0.59344 | 0.36795 |